In: Monomers, Oligomers, Polymers, Composites… ISBN: 978-1-60456-877-6
Editors: R. A. Pethrick, G.E. Zaikov et al.

Chapter 13

A THEORETICAL APPROACH FOR PREDICTION OF YARN STRENGTH IN TEXTILE INDUSTRY

A.Shams-Nateri and A.K.Haghi*
University of Guilan, P. O. Box 3756, Rasht, Iran

ABSTRACT

This paper describes advance techniques that can be used to predict ring spun yarn strength from HVI/FMT measured properties of cotton fibers such as span length, bundle strength, fineness, uniformity ratio and maturity of cotton fibers. Neural networks, neuro-fuzzy, multiple-linear regression techniques and Sitra's expressions were used to predict yarn strength from cotton fibers properties. The results of intelligence system were better than multiple-linear regression techniques and Sitra's expressions. The best results were obtained by neuro-fuzzy method.

Keywords: Cotton, Fiber, Yarn, Relationship, Regression, Neural Network, Neuro-fuzzy

INTRODUCTION

One of the most important production processes in the textile industry is the spinning process, which started with cotton fiber. Yarn has been produced in rotor or ring spinning machine. The quality of the resulting yarns is very important in determining their application possibilities. The two most important characteristics of yarn are its tenacity and elongation. Prediction formulae to related fiber properties to yarn quality have been an interesting field of work for several research workers for more than three decades [1, 2].

Sitra was developed expressions for prediction yarn strength from fiber properties in the year 1989[3]. In the prediction expressions fiber properties measured with conventional instrument. In next step, they establish prediction expressions for strength of spun yarns from

* Corresponding author: Haghi@Guilan.ac.ir

cotton fiber properties using HVI test system. The following expression was derived for yarn Lea CSP under good working condition for carded count:

$$Lea \cdot CSP = 280 \times \sqrt{FQI} + 700 - 13C \quad (1)$$

In addition, And for combed count:

$$Lea \cdot CSP = (280 \times \sqrt{FQI} + 700 - 13C) \times (1 + \frac{W}{100}) \quad (2)$$

Where FQI is fiber quality index and arrived from the following formula:

$$FQI = \frac{L \times S \times m}{F} \quad (3)$$

Where

L: 50% span length (mm)
S: Bundle strength (g/tex)
F: Fineness (micronnaire value)
m: Maturity
C: Yarn count (Ne)
W: Percentage waste extracted during combing

If the maturity coefficient values are not readily available, as a rough approximation the yarn CSP values may be arrived from the following formula:

$$Lea \cdot CSP = 250 \times \sqrt{\frac{LS}{F}} + 590 - 13C \quad (4)$$

For yarn strength, RKm value defined as:

$$RKm = \frac{Single\ Yarn\ strength}{Tex\ Count\ of\ Yarm} \quad (5)$$

RKm value can be predicted from CSP value by following formula:

$$RKm = \frac{Lea.CSP}{150} \quad (6)$$

Chellamani et al. reported a similar relationship between fiber properties and yarn strength [4]. The relationship between the yarn strength and fiber properties was studied and a

Fiber Quality Index was derived to overcome inconsistencies within the basic fiber properties. Then, it was used to predict the strength of the yarn and significant correlations were obtained.

This work reports a new method for prediction ring spun yarn strength from cotton fiber properties by intelligence system such as neural network and neuro-fuzzy methods.

NEURAL NETWORK

Recently, many researches have utilized a parallel processing structure that has a large number of simple processing structures that has a large number of simple processing with many interconnections between them [5-8]. The use of these processors is much simpler and faster than one central processing unit (CPU). Because of recent advantages in VLSI technology, the neural network has emerged as a new technology and has found wide application in many areas (as well).

In this work, the multi-layer perceptron was used to process data by using the modified back-propagation algorithm. This algorithm attempt to minimize an error function Φ by modification of network connection weights and bias. The parameters of Φ are the weights of network and its value is error measure.

In each iteration an input vector is presented to the network and propagated forward to determine the output signal. The output vector is then compared with the target vector resulting an error signal, which is backed propagated through the network in order to adjust the weights and bias. This learning process is repeated until the network respond for each input vector with an output vector that is sufficiently close to the desired one. The general formula for the output of each unit in the network (except for the input units) is given by:

$$y_{i,l} = \varphi\left(\sum_{j=1} \omega_{ij,l} \times y_{j,l-1} + b_{i,l}\right) \tag{7}$$

Where j runs over all nodes of $(l\text{-}1)^{th}$ layer and $\omega_{ij,l}$ is the strength of the coupling between unit I in l^{th} layer and unit j in the previous layer, $y_{j,l-1}$ is the activation of j^{th} unit in $(l\text{-}1)^{th}$ layer, and $b_{i,l}$ is the bias for unit I in l^{th} layer. $\varphi(.)$ Is the nonlinear activation function which can be log-sigmoid (logistic sigmoid), hard limiting, etc., but usually the log-sigmoid function is used, $\varphi(s)=1/91+e^{-s}$).

At each iteration, the values of the weights are modified in the direction in which the error function should decrease most rapidly. The direction and magnitude of the modification is given by the gradient of the error function with proportionality commonly referred to as the learning rate or step size. The formula is, [8]:

$$\omega_{ij}^{n=1} = \omega_{ij}^{n} + \Delta\omega_{ij}^{n} \tag{8}$$

$$\omega_{ij}^{n=1} = \omega_{ij}^{n} - \eta \frac{\partial \phi^{n}}{\partial \omega_{ij}^{n}} \tag{9}$$

Where ω_{ij}^{n} is the interconnection weight between the i^{th} unit in any layer and j^{th} unit in the previous layer in the n^{th} iteration. ϕ^{n} is the error function of network at the n^{th} iteration, and η is the learning rate.

The computation of partial derivatives is described in what follows in some detail. In the general back-propagation method, Φ is defined as the sum of the squared error for all output nodes:

$$\phi = E_{\Sigma} = \|E\|^2 = \|O - T\|^2 = \sum_{i=1}^{N0} (O_i - t_i)^2 \tag{10}$$

where N_0 is the number of the output nodes. Therefore, the partial derivative of the sum of the squared error, E_{Σ} , with respect to w is given by:

$$\frac{\partial E_{\Sigma}}{\partial W} = \frac{\partial E_{\Sigma}}{\partial O} \times \frac{\partial O}{\partial X} \times \frac{\partial X}{\partial W} = 2 \times E \times O \times (1 - O) \times Y' \tag{11}$$

Where *w* is the weights between the last hidden layer and the output layer.

Since, the original back-propagation method converges slowly, the new method used to speed convergence. In this method, the new function Φ is designed that is given by [9,10]:

$$\phi_{new} = (1-T)^{n} \times \left[\log_e(s) - \log_e(1-s)\right] + \sum_{j=1}^{p} \left\{ \begin{array}{l} \left(\prod_{i=0}^{j-1} (m-i)\right) \frac{(1-T)^{m-j}}{j!} .(-1)^{j} \\ \left[\log_e(s) - \binom{j}{1} S + \binom{j}{2} \frac{s^2}{2} + \ldots + \right] \\ (-1)^{r} . \binom{j}{r} \frac{s^{r}}{r} + \cdots + (-1)^{j} . \frac{s^{j}}{j} \end{array} \right\} \tag{12}$$

$$\forall \begin{cases} s = O \quad \text{if} \quad E \rangle 0 \\ s = 2T - O \quad \text{if} \quad E < 0 \end{cases}$$

To minimize where followed to:

$$\frac{\partial \phi}{\partial W} = \frac{\partial \phi}{\partial O} \times \frac{\partial O}{\partial X} \times \frac{\partial X}{\partial W} = sign(E).\left|E\right|^{m} \times Y' \tag{13}$$

The approach of this algorithm is much faster than the other ones designed and provided the better performance

ANFIS

The fuzzy inference system (FIS) is a popular computing framework based on the concepts of fuzzy set theory, fuzzy IF/THEN rule and fuzzy reasoning to transform an input space into an output space. The basic structure of fuzzy inference system consists of three conceptual components:

1. A rule base
2. Database or dictionary which defines the membership functions used in the fuzzy rules
3. Reasoning mechanism, which performs the inference procedure upon the rule and a given condition to derive a reasonable output or conclusion.

A fuzzy system can be created to match any set input/output data. This can be done with an adaptive neuro-fuzzy inference system (ANFIS). ANFIS is about taking a fuzzy inference system and training it with a backpropagation algorithm, well known in the artificial neural network (ANN) theory, based on some collection of input/output data[11,12,13,14].

ANFIS consist of a Takagi Sugeno FIS and has a five layered as shown in figure 1. The first hidden layer is for fuzzification of the input and T-norm operators are positioned in the second hidden layer to compute the rule antecedent part. The third hidden layer normalizes the rule strengths followed by the fourth hidden layer where the resultant parameters of the rule are determined. Output layer computes the overall input as the summation of all incoming signals. ANFIS uses backpropagation learning algorithm to determine premise parameters (to learn the parameters related to membership functions) and least mean square estimation to determine the consequent parameters. A step in the learning procedure has two parts: In the first part, the input data are propagated, and the best consequent parameters are estimated by an iterative least mean square method, while the premise parameters are assumed to be fixed for the current cycle during the training set. In the second part, the patterns are propagated again, and in this epoch, backpropagation is used to modify the argument parameters, while the resulting parameters remain fixed. This method is then repeated. The fuzzy inference system is known by numerous other names, such as fuzzy-rule-based system, fuzzy expert system, fuzzy model, fuzzy associative memory, fuzzy logic controller and simply fuzzy system [15, 16, and 17].

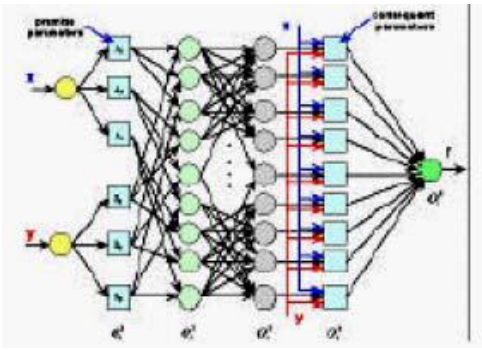

Figure 1. Structure of ANFIS.

EXPERIMENTAL

In this work, 22 variety quality cotton fibers samples were selected for making relation between cotton fibers properties and yarn quality. The cotton fiber properties such as spun length, fiber bundle strength, maturity; micronnaire was measured by HVI/FMT system. Ring spun yarn was spun in Rieter spinning system and their quality was measured. The properties of cotton fiber and quality of spun yarn are shown in tables 1.

Table 1. Cotton fibers Properties and yarns quality

Sample No.	Yarns quality		Cotton fibers properties			
	Count (Ne)	RKm	50% span length (mm)	Micronnair	Maturity ratio	Fiber bundle Strength (g/tex)
1	41	14	14	2.69	0.46	20.21
2	39	16.95	13.54	4.6	0.86	23.38
3	40.2	16.56	13.83	4.04	0.82	18.47
4	40.2	17.6	13.76	3.79	0.87	17.99
5	39.5	14.57	11.57	3.79	0.88	20.88
6	39.8	15.37	13.03	3.47	0.75	21.11
7	40.6	16.24	13.48	4.53	0.86	22.86
8	40	14.47	13.38	3.39	0.66	16.65
9	40.7	17	13.17	3.34	0.66	16.28
10	40	16.3	14.77	3.69	0.81	19.77
11	39.9	15.4	13.78	3.55	0.82	18.86
12	39	15.8	12.6	3.21	0.72	19.58
13	39.2	15.7	14.37	5.19	0.9	18.54
14	40	15.07	13.38	3.61	0.72	18.58
15	29.8	16.04	13.3	3.04	0.54	19.99
16	24	13.9	13.97	3.58	0.66	19.26
17	29.5	14.78	13.41	3.06	0.6	19.42
18	29.3	15.96	13.26	3.33	0.63	19.36
19	38.8	15.47	13.72	3.48	0.69	19.64
20	40.4	14.36	14.76	3.56	0.76	20.2
21	40.6	14.43	13.82	3.84	0.64	19.69
22	28.9	16.7	14.72	4.31	0.86	20.4

RESULTS AND DISCUSSIONS

At first, the relationship between fiber properties and strength of spun yarn was study by using Sitra's expression (Equation 1). The predicted value of yarn RKm for various samples is given in table 2. in second method, two multiple linear regressions was used to correlate yarn strength to cotton fiber properties. In first method of regression, Lea CSP of yarn was calculated from 50% span length (L), Bundle strength(S), Fineness (F), Maturity(M) of cotton fibers and yarn count (C) by Equation 14:

$$RKm = 9.73 + 0.229 \times L - 0.08 \times F + 3.7 \times M - 0.027 \times S + 0.0249 \times C \qquad (14)$$

In second method, RKm value of yarn was calculated from fiber quality index (FQI) and yarn count (C) by equation 15:

$$RKm = 12 + 0.0527 \times C + 0.0308 \times FQI \qquad (15)$$

In neural network technique, network has two input nods, one output nod and two hidden layers respectively with 4 and 2 nods. Two input nods referred to fiber quality index (FQI) and yarn count and one output nod referred to yarns strength. Neural network training was continued over 1000 epochs by back propagation algorithm. After training, the neural network was tested with all sample. The results of yarns strength prediction are given in tables 2 and 3.

In neuro-fuzzy method, ANFIS system applied to prediction yarns strength from cotton fibers properties. ANFIS system was designed with two input, 81 IF-THEN rule and one output (figure 2). Two input nods referred to fiber quality index (FQI) and yarn counts. One output nod referred to spun yarn strength. First input had three Gaussian shape membership function and second input had four Gaussian shape membership function. Network was trained by back-propagation algorithm. After training, the ANFIS was tested with all samples. The predicted results are shown in tables 2 and 3.

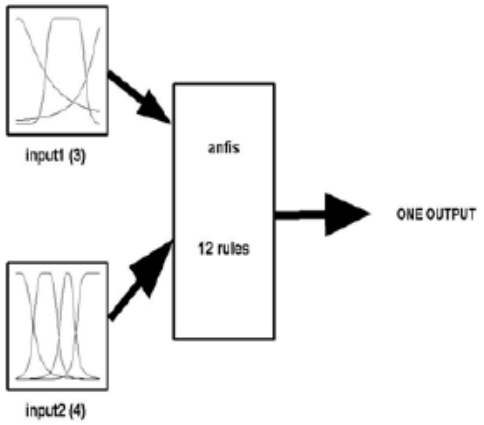

Figure 2. The ANFIS system structure.

Table 2. Actual and predicted RKm value of ring spun yarns

Sample No.	Actual Value	Regression Method I	Regression Method II	Sitra Method	Neural network Method	Neuro-fuzzy Method
1	14	14.90	15.65	14.76	13.88	14.00
2	16.95	15.98	15.88	16.31	16.83	16.95
3	16.56	16.11	15.72	15.29	16.66	16.56
4	17.6	16.31	15.87	15.92	16.96	17.60
5	14.57	15.75	15.81	15.89	15.87	14.57
6	15.37	15.63	15.93	16.28	15.38	15.41
7	16.24	16.03	15.94	16.09	16.25	16.24
8	14.47	15.51	15.44	14.16	14.46	14.47
9	17	15.49	15.45	13.96	17.02	17.00
10	16.3	16.28	16.08	16.81	16.31	16.30
11	15.4	16.12	15.95	16.34	15.3	15.36
12	15.8	15.47	15.76	15.84	15.21	15.78
13	15.7	16.41	15.49	14.62	15.75	15.70
14	15.07	15.66	15.64	15.01	14.99	15.07
15	16.04	14.73	15.03	15.58	16.12	16.05
16	13.9	15.16	14.79	16.40	13.92	13.90
17	14.78	14.99	15.13	16.12	14.84	14.78
18	15.96	15.04	15.04	15.80	15.96	15.95
19	15.47	15.58	15.69	15.61	15.2	15.48
20	14.36	16.10	16.09	16.72	14.37	14.00
21	14.43	15.43	15.54	14.39	14.41	16.95
22	16.7	16.11	15.37	17.28	16.73	16.56

Table 3. The absolute error of yarns strength prediction

No.	Methods	Mean	SD	Max	Min
1	Sitra	5.960	5.551	17.986	0.253
2	Regression	5.594	3.449	12.047	0.253
3	Regression	5.108	3.205	12.117	0.123
4	Neural network	1.069	2.043	8.922	0
5	Neuro-fuzzy	0.984	3.721	17.464	0

CONCLUSIONS

In this chapter, Intelligence System was used to prediction ring spun yarns strength from cotton fiber properties and compared with conventional method. The ring spun strength was predicted from HVI/FMT measured properties of cotton fibers such as span length, bundle strength, fineness, uniformity ratio and maturity. The fiber quality index (FQI) was defined from 50% span length, Bundle strength , Fineness (micronnaire value), Maturity of cotton fibers. The FQI, as a quality parameter of cotton fiber, was used in making relationship between yarns strength and cotton fibers properties. Several methods such as neural networks, neuro-fuzzy and multiple-linear regression techniques and Sitra's expressions were used to

predict yarns strength. The results conclusively prove the superiority of intelligence system over multiple-linear regression techniques and Sitra's expressions. The best results was achieved by neuro-fuzzy method.

REFERENCES

[1] Sette, S.; L. Boullart ; L. Van Langenhove and P. Kiekens 1997. " Optimizing the Fiber-to-Yarn Production Process With a Combined Neural Network/Generic Algorithm Approach". *Textile Research Journal*, 67(2), 84-92.

[2] Ramey H.H. ; R. Lawson R. and S.Worley 1977. " Relationship of Cotton Fiber Properties to Yarn Tenacity". *Textile Research Journal*, 47(10), 685-691.

[3] Chellmani K.P. ; K. Gnanasekar ; M.S. Ravindran and T.V. Ratnam 1995. " Fiber Yarn Relationships Using HVI/FMT Measured Fiber Properties". The South India Textile Research Association (SITRA), Vol.41, No. 1.

[4] Chellamani P. ; Indra Doraiswamy; T.V. Ratnam 1990. " Fiber Quality and Yarn Strength Relationships". *Indian Journal of Fiber & Textile Research*, Vol. 15, 1-5.

[5] Bishop J.M. , Bushnel M.J. and Westland S., " Application of Neural Networks to computer recipe Prediction", *Color Res. Appl. J.* 16,(1991)

[6] Westland S.,"Advances in Artificial Intelligent for the Color Industry", *J. Soc. Dyers Color*, 110, (1994), 370-375.

[7] Amirshahi S.H., Roushan_Zamir J.M. and Torkamani-Azar F.,"An Attempt to Application of Neural Networks in Recipe Prediction", *Int. J. Eng. Science*, 11, (200), 51-59.

[8] Rumelhart G. E., Hilton G.E. and Williams R.G.," Learning Internal Representation by Error Propagation, in: Parallel Distributed Processing", Vol.1, Chp. 8, Cambridge, MA, MIT. Press, (1986).

[9] Torkamani-Azar F. "Comparative studies of Diffusion Equation Image Recovery Methods with an Improved Neural Network Embedded Technique" PhD Thesis, The University of New South Wales, (Jan. 1995).

[10] Torkamani-Azar F.,"A Modified Back Propagation Algorithm", Second Annual Computer Society of Iran Conference, Tehran,(Dec. 1996), 217-226.

[11] Marjoniemi M. and E. Mantysalo 1997. " Neuro-Fuzzy Modeling of Spectroscopic Data. Part A: Modeling of Dye Solutions". *J.S.D.C.*, Vol.113, 13-17.

[12] Marjoniemi M. and E. Mantysalo 1997. " Neuro-Fuzzy Modeling of Spectroscopic Data. Part B: Dye Concentration Prediction", *J.S.D.C.*, Vol.113, 64-67.

[13] Jang J.S.R. 1993. " ANFIS: Adaptive-network-based fuzzy Inference System". *IEEE Trans. On Sys., Man.* Cyb., 23.

[14] Nariman-Zadeh N. and a. Darvizeh 2001. " Design of Fuzzy System for the Modeling of Explosive Cutting Process of Plates Using Singular Value Decomposition". WSES 2001 Conf. On fuzzy sets and fuzzy systems (FSFS, 01) , spain(Feb).

[15] Jang R, *Neuro-Fuzzy Modeling: Architectures, Analyses and Applications*, PhD Thesis, University of California, Berkeley, July 1992.

[16] A. Abraham, "Neuro Fuzzy Systems: State-of-the-art Modeling Techniques", http://ajith.softcomputing.net,2007.

[17] J.S.R. Jang, C.T. Sun, E. Mizutani, "Neuro fuzzy and Soft Computing" , The Prentice-Hall, Inc. USA, 1997.

In: Monomers, Oligomers, Polymers, Composites… ISBN: 978-1-60456-877-6
Editors: R. A. Pethrick, G.E. Zaikov et al.

Chapter 14

TECHNOLOGICAL ADVANCES IN GEOTEXTILES

A.H. Tehrani and A. K. Haghi*
University of Guilan, P. O. Box 3756, Rasht, Iran

ABSTRACT

According to the need and ascendant approach of technical textiles and the absence of its technical application as respect to the construction industry, this chapter is intended to provide a comprehensive and critical review on geotextiles. This should be of value to those interested in civil, chemical, textile and polymer engineering.

1. ABRASION RESISTANCE OF THERMALLY BONDED 3D NONWOVEN FABRICS

Employing the established standard Martindale abrasion method, the abrasion resistance of the three-dimensional nonwoven filter sample produced using the recently developed air laid web formation process and through-air thermal bonding process and the commercially available polypropylene (PP)/polyester (PET) (sheath/core) bi-component staple fiber as raw material, has been evaluated. Results obtained indicated that there are two failure forms for the thermally bonded nonwoven samples during the abrasion testing, the peeling of the fiber PP sheath and the pilling forming and breaking off. The process parameters, including the bonding temperature, dwell time and hot air velocity and fabric weight clearly affect the abrasion resistance of the thermally bonded nonwoven filter samples. These effects could be correlated with the thermal oxidative degradation of the fiber PP sheath during the thermal bonding process and the compactness of the resulting samples.

* Corresponding author e-mail: Haghi@Guilan.ac.ir

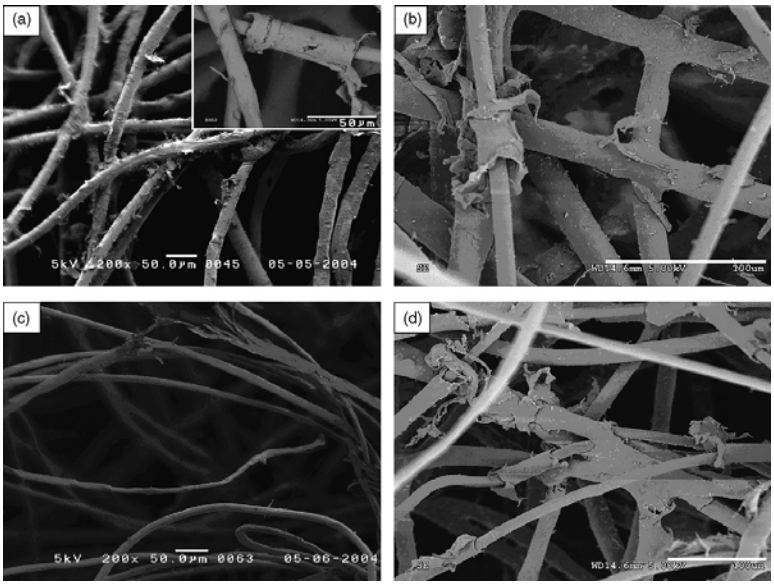

Figure 1. SEM images showing the development of the peeling and wearing away of the PP sheath of the bi-component fiber during the abrasion testing for the thermally bonded nonwoven samples: (a) BT4, surface wear and lifting, the inset shows the details of fiber peeling; (b) AD1, broken fragments of fibers, surface peeling and breakdown of fibers; (c) IV1, fiber failure by multiple splitting or breakage; (d) DT3, peeling away of large pieces.

Technological advances (figures 1-4) in the textile industry have resulted in an ongoing demand for cost-effective processing techniques and textiles. In the past 40 years, nonwoven techniques and products have been developing and growing at a phenomenal rate, corresponding to such a demand [1-6]. The most significant feature of nonwoven fabrics, and also the one that contributes most to their economical appeal, is that the fabrics are usually made directly from raw materials in a continuous production line, thus partially or completely eliminating conventional textile operations, such as carding, roving, and spinning, weaving or knitting. The simplicity of fabric formation, coupled with high productivity, allows nonwovens to compete favorably with woven's and knits on a performance per cost basis in many industrial applications, from simple low cost replacements for more expensive textiles to high-quality textiles and many functions that could never be filled by regular textiles.

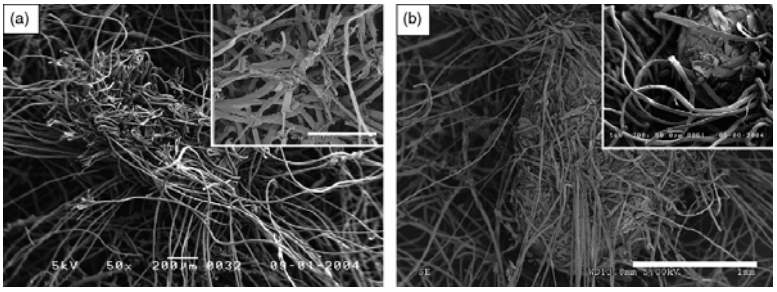

Figure 2. SEM images show (a) the early stage of pill development; (b) the fiber entanglement, splitting and well-developed pill during the abrasion testing for the thermally bonded nonwoven sample DT3. The insets in both images present the details under higher magnification.

Over the past few decades, the overwhelming majority of the research is related to the manufacture and use of nonwovens as essentially two-dimensional (2D) sheet structures. In many applications where three-dimensional (3D) fibrous web structures are needed, they have to be constructed from the flat sheet fabrics. If 3D nonwoven shell structures are produced in a single process, directly from fibers, the packaging, freight and labor costs and the cost of wastage inevitably generated during panel cutting can be saved possibly up to 70% of the production cost.

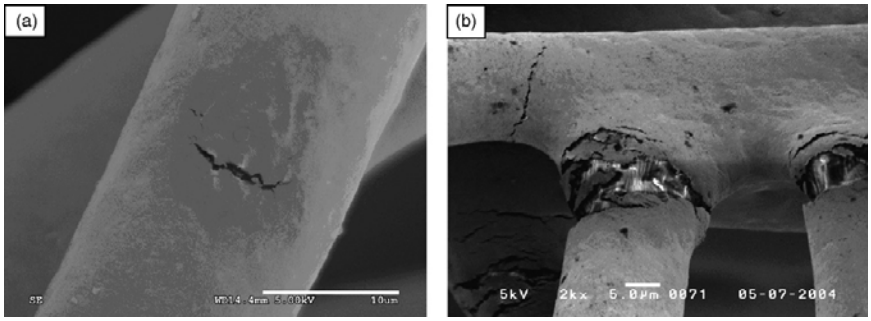

Figure 3. SEM images showing the cracks on the fiber surface of the thermally bonded nonwoven sample: (a) BT1 and (b) BT4.

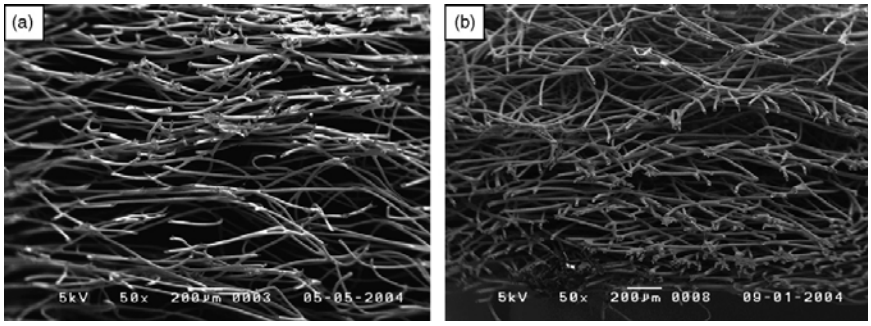

Figure 4. SEM images taken from the cross sections of the thermally bonded nonwoven samples: (a) IV1 produced using the hot air velocity 1.5 m/s and (b) IV3produced using the hot air velocity 4 m/s.

It can also shorten the process and save equipment investment, space and energy. However, 3D shell structure nonwovens are still at the very beginning stage of development. Major difficulties for manufacturing of 3D shell structure nonwovens (figure 5) arise in web formation and web solidification. This is because it is much more difficult to manipulate and control the fiber distribution and bonding of a 3D shell structure web than do those of a 2D web, aiming to achieve nearly uniform and orientation random fiber distribution, and, hence, uniformity and isotropic properties of the final product[7-11]. Up to date, there have been only a few reports on the production of 3D nonwoven structures. Recently, a pilot process to air-form 3D nonwoven fabrics, using the air laid web formation process and through-air bonding technique, has been developed. Samples of the hats prepared using this process have been proved to be remarkably even and strong, and are about to be commercialized by the only chef's hat producer in the UK who previously sponsored the research work. The

principles of this process were promising and further studied in the present work for a variety of other products, especially filters, finger-shaped towel and garment interlinings, e.g., bra cups.

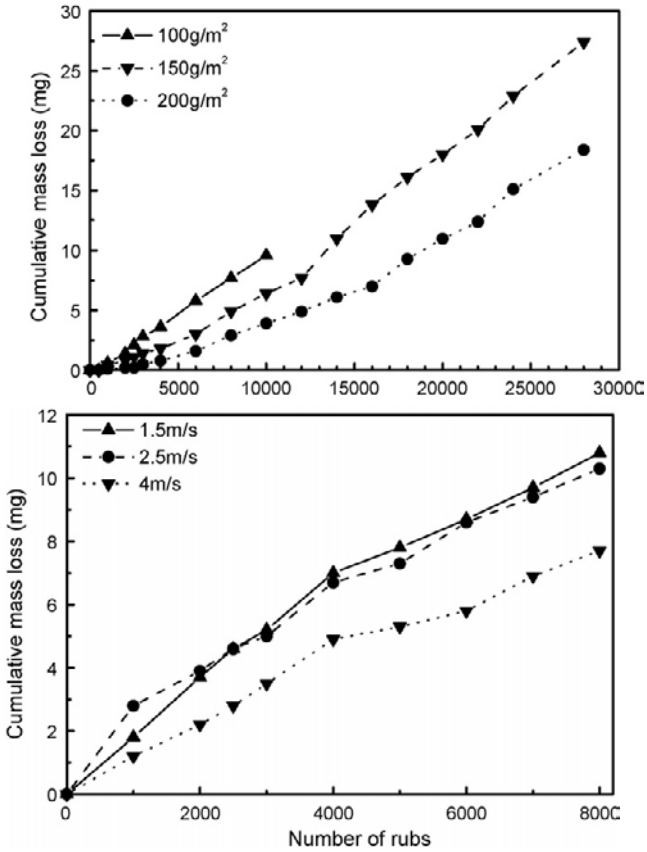

Figure 5. Cumulative mass losses of nonwoven fabrics produced using different hot air velocities and Cumulative mass losses of nonwoven fabrics with and different fabric area densities.

As the conclusion the abrasion resistance of the 3D nonwoven filter samples, produced using the air laid web formation process and through air thermal bonding process, has been evaluated using the established standard Martindale abrasion method. The effects of the bonding temperature, dwell time, air velocity and fabric weight on the abrasion resistance were considered and the following conclusions can be drawn:

1. SEM examination reveals that there are two failure forms for the thermally bonded nonwoven samples during the abrasion tests, the peeling of the fiber PP sheath, and the pilling forming and breaking off.
2. The abrasion resistance of the thermally bonded nonwoven fabrics decreases with increasing the thermal bonding temperature. This can be attributed to the fact that more mechanical defects, such as cracks, may be formed resulting from a higher lever of the thermal oxidative degradation and a higher amount shrinkage of the PP sheath of the fiber at a higher bonding temperature.

3. The abrasion resistance of the nonwoven fabrics increases up to a maximum, and, then, decreases with further increasing the dwell time. The poor abrasion resistance of a nonwoven fabric produced using a shorter dwell time can be ascribed to the under-bonding between the fibers. The poor abrasion resistance of a nonwoven fabric produced using a longer dwell time may be due to a higher lever of the thermal oxidative degradation of the PP sheath, resulting in the peeling and multiple splitting of the PP sheath more serious.
4. The abrasion resistance of the thermally bonded nonwoven samples is also significantly affected by the hot air velocity and the fabric weight. It increases with the increasing both the hot air velocity and the nonwoven fabric weight. This can be due to the fact that the thermally bonded nonwoven samples become more compact with the increasing both the hot air velocity and the fabric weight, hence leading to the higher abrasion resistance.
5. The effects of the bonding temperature, dwell time, air velocity and fabric weight on the abrasion resistance indicate that the various process parameters are all critical for achieving the most abrasion-resistant fabric.

2. INTERNAL DEFORMATION BEHAVIOR OF GEOSYNTHETIC-REINFORCED SOIL WALLS

Local deformation of geosynthetics, such as Geogrids, and nonwoven and woven geotextiles, was measured to analyze the stability of geosynthetic-reinforced soil (GRS) structures. To analyze the deformation behavior of geosynthetics applied to a reinforced soil structure, the tensile load–elongation properties of the geosynthetic and local deformation measurement data are required. However, local deformation of nonwoven geotextile (NWGT), which is permeable, is difficult to measure with strain gauges. This study proposes a new, more convenient, method to measure the deformation behavior of NWGTs using a strain gauge and examines its suitability via laboratory tests and field trials on two GRS walls. A wide-width tensile test, conducted under a confining pressure of 70 kPa, showed that local deformation of NWGT, measured with strain gauges of type AE-11-S80N-120-EL, was similar to total deformation measured with linear variable deformation transformer (LVDT). In field trials, NWGT showed a larger deformation range than woven geotextile or Geogrids. However, the deformation patterns of the three materials were similar. The strain gauges attached to NWGT in the walls worked normally for 16 months. Therefore, the method proposed in this study for measuring NWGT deformation using a strain gauge was effective and valuable. Pore water pressure in the GRS wall can be ignored since the backfill remains unsaturated regardless of rainfall. However, it should be noted for design purposes that horizontal earth pressures at the wall face are greater at the bottom and top of the wall than at rest.

Reinforced walls have been the subject of considerable research, and a number of recent papers have examined different aspects of their design and behavior Owing to the increasing need for clayey soil (CL) as backfill in reinforced soil walls, nonwoven geotextiles (NWGTs) with drainage capability have received attention. NWGTs have the merit of high drainage capability and low cost, but also have a drawback of low tensile stiffness and higher

deformability than Geogrids or woven geotextiles. To analyze the deformation behaviors of reinforcements, load–elongation properties and local deformation measurement data are needed; however, measuring local deformations of GRS walls in the field is problematic. It is suggested using silicon to attach strain gauges to the woven geotextile.

Strain gauges can be attached directly to woven geotextiles and Geogrids (however, it is not easy to measure deformation of NWGTs by direct attachment of strain gauges because the gauges separate from the surface of NWGTs to which they are attached as NWGTs are elongated by a tensile force. A method of attaching strain gauges to the surface of NWGT composed of a core layer of knitted textile and needle-punched double layer of NWGT, by using gauge cement (Kyowa, EC-30). This study examines an easy method, using an adhesive, to attach strain gauges to NWGTs, and the applicability of the technique via laboratory and field tests. To analyze deformation behavior of reinforcements within GRS walls, two 5-m walls were constructed on a weak, shallow-layered foundation and fitted with a compound arrangement of NWGTs/woven geotextiles and nonwoven/Geogrids. Deformation behavior inside the GRS walls was analyzed using data collected from four earth-pressure gauges, four pore-water pressure gauges, and 124 strain gauges attached to NWGTs and woven geotextiles and Geogrids reinforcements over a period of about 1.5 years.

As a conclusion a laboratory wide-width tensile test conducted under a confining pressure of 70 kPa showed that the pattern of local deformation on NWGT measured with strain gauges resembled that of the total deformation measured with LVDT. In GRS walls, NWGT showed a larger deformation range than the woven geotextile or Geogrids. However, deformation patterns of these three reinforcement materials were similar and the strain gauges attached to the geosynthetics functioned normally for 16 months. Therefore, the method of measuring a NWGT deformation by using a strain gauge, as suggested by this study, was effective. The backfill material probably remained unsaturated regardless of rainfall because there were no signs of drainage through NWGT from the backfill, and the pore water pressures throughout the measurement period showed negative values. Therefore, pore water pressures in the wall can be ignored. However, horizontal earth pressures at the wall face were larger at the bottom and top of the wall than earth pressures at rest. Therefore, when a GRS wall with a flexible wall face is constructed on a shallow, weak foundation, as in this study, precautions must be taken during the design and construction of the wall, since the horizontal earth pressure can be larger than earth pressure at rest at the bottom of the wall.

3. COMPARATIVE STUDY BETWEEN NEEDLE PUNCH NONWOVEN GEOTEXTILE STRUCTURES MADE FROM FLAX AND POLYESTER FIBERS

Geotextiles are widely used in civil and geotechnical engineering applications. In this study, a comparison is made between the properties of the needle punched nonwoven geotextiles produced from polyester and flax fibers. The properties of geotextiles including density, pore size and permeability have been investigated. It has been found that large inherent variation in flax fiber length and fineness can result in loss of tensile strength and cause large variation in smallest detected pore diameter. Nevertheless, flax fiber-based geotextiles have a great potential in various civil engineering applications as they are found to

be less anisotropic, more compact and have produced an ‘‘open structure’’. Furthermore, the influence of process parameters, namely feed rate, stroke frequency and depth of needle penetration, on the properties of the geotextiles has been observed. Geotextiles are woven, knitted or nonwoven structures, widely used in civil engineering applications and are a core member of geosynthetic family. Recently, there has been an ever-increasing interest in nonwoven geotextiles as these structures are simple, flexible and can be produced at a lower cost. It is essential that the geotextile structures should be able to fulfill more than one function, i.e. separation, drainage and filtration. The design of a geotextile accounts for soil–geotextile interaction, internal stability of the soil, isotropic characteristics of the geotextile structure and flow conditions, i.e. seepage velocities and hydraulic gradients.

Comparison of tensile properties of geotextiles produced from flax and polyester fibres

Sample ID	Tensile strength in machine direction (TMD) (N/50 mm)		Tensile strength in cross-machine direction (TXMD) (N/50 mm)		TXMD/TMD	
	Polyester	Flax	Polyester	Flax	Polyester	Flax
G1	107.05	58.20	164.88	83.0	1.54	1.43
G2	168.08	75.20	287.04	118.2	1.71	1.57
G3	156.44	43.80	220.56	52.2	1.41	1.19
G4	241.90	99.00	386.78	91.0	1.60	0.92
G5	139.32	70.68	225.48	68.56	1.62	0.97
G6	197.48	99.84	348.32	124.8	1.76	1.25
G7	167.82	57.40	248.54	68.8	1.48	1.20
G8	284.48	104.16	455.92	135.4	1.60	1.30
G9	289.10	113.04	467.8	148.1	1.62	1.31
G10	147.04	55.80	227.04	65.2	1.54	1.17
G11	234.24	76.80	344.22	114.4	1.47	1.49
G12	116.40	85.40	208.94	134.6	1.80	1.58
G13	253.34	84.60	388.76	93.91	1.53	1.11
G14	128.08	91.92	198.72	113.06	1.55	1.23
G15	224.62	83.04	367.02	119.57	1.63	1.44

However, the selection of fiber and fabric types is of paramount importance for any geotextile-based application. The advantages of natural fibers are robust, superior strength/durability properties, good drape ability and biodegradability/ environment friendliness but these fibers are biocompatible. Nevertheless, several researchers have reported the use of natural fibers including jute, coir, wood and bamboo in various applications such as soil erosion control, vertical drains, road bases, bank protection and slope stabilization.

Therefore, the overall objective of the present work is to compare and analyze the properties of needle punched nonwoven geotextiles produced from flax and polyester fibers under the similar process conditions. Fifteen samples of needle punched nonwoven geotextile structures were produced from each polyester and flax fiber by employing a central composite experimental design as shown in table 1. The fineness and length of fiber samples were normalized to 6 dtex and 60 mm, respectively. However, the coefficients of variation in fineness and length of the flax fiber were found to be 25.35% and 26.85%, respectively. The needle punched nonwoven geotextile structures were produced by initially opening the staple

fiber bale by carding and subsequently orientated to cross-machine direction using a cross-lapper to form a web of required area density. Following the production of the needle punched nonwoven fabrics, standard tests were performed on the fabrics to determine their area density (ASTM D3776, 1996), thickness (ASTMD5729, 1995), the pore size (ASTM E1294, 1999), and water permeability (EN ISO 11058, 1999).

Comparison of dimensional properties of geotextiles produced from flax and polyester fibres

Sample ID	Fabric weight (g/m^2)			Fabric thickness (mm)			Fabric density (g/cm^3)		
	Polyester	Flax	Polyester/flax	Polyester	Flax	Polyester/flax	Polyester	Flax	Polyester/flax
G1	284.2	128.3	2.22	3.32	1.66	2.00	0.0856	0.0773	1.11
G2	407.6	170.4	2.39	4.46	2.08	2.14	0.0914	0.0819	1.12
G3	261.6	93.8	2.79	2.94	1.17	2.51	0.0890	0.0804	1.11
G4	372.3	165.0	2.26	3.77	2.59	1.46	0.0987	0.0890	1.11
G5	259.6	117.8	2.2	2.7	1.32	2.05	0.0962	0.0637	1.51
G6	366.3	166.4	2.2	3.55	1.91	1.86	0.1032	0.0872	1.18
G7	236.1	112.8	2.09	2.37	1.25	1.9	0.0996	0.0869	1.15
G8	339.1	173.6	1.95	3.00	1.99	1.51	0.1130	0.0903	1.25
G9	363.9	188.4	1.93	3.85	2.15	1.79	0.0945	0.0874	1.08
G10	228.7	93.0	2.46	2.48	0.99	2.51	0.0922	0.0942	0.98
G11	263.7	128.0	2.06	2.85	1.48	1.93	0.0925	0.0864	1.07
G12	296.3	145.0	2.04	3.47	1.74	1.99	0.0854	0.0835	1.02
G13	303.6	141.0	2.15	2.77	1.86	1.49	0.1096	0.0757	1.45
G14	312.4	153.2	2.04	3.61	1.99	1.81	0.0865	0.0767	1.13
G15	307.6	138.4	2.22	3.26	1.83	1.78	0.0944	0.0755	1.25

As a conclusion a comparison is made between the properties of the needle punched nonwoven geotextiles produced from flax and polyester fibers using the same experimental matrix. Polyester fiber-based geotextiles are found to be dense corresponding to the flax fiber-based geotextiles due to high elastic recovery of polyester fiber. Although the fibers in the nonwoven structure were preferentially orientated in the cross-machine direction, the flax fiber-based geotextiles resulted in loss of tensile strength in the cross-machine direction (sample IDs G4 and G5) due to large inherent variation in length and fineness of the flax fiber. This has also led to the large variation in the smallest detected pore diameter in flax fiber geotextiles in comparison to the polyester fiber-based geotextiles. Nevertheless, flax-based geotextiles are found to be more compact and less anisotropic in nature. In addition, flax fiber geotextiles have produced an ‘‘open structure’’ at a lower FR, moderate SF and depth of NP (sample ID G10).

4. Dynamic Studies of Polypropylene Nonwovens in Environmental Scanning Electron Microscope

Environmental scanning electron microscopy (ESEM) provides new tools to examine the dynamic behavior of various materials under different conditions. The dynamic experiments of water wetting, oil sorption and loading deformation of polypropylene (PP) nonwovens in the ESEM were studied in this paper. Water wetting tests were performed by controlling the temperature of the specimens and chamber pressure in favor of water condensation at 100% relative humidity. The wetting by oil was made using a micro-injector to add oil droplets onto specimens being observed. The ESEM observations revealed the contrast in the wetting behavior of the PP nonwovens towards water and oil. Tensile testing experiments were performed in the ESEM using a tensile stage. The dynamic studies gave new insight into microscopic behavior of PP nonwovens.

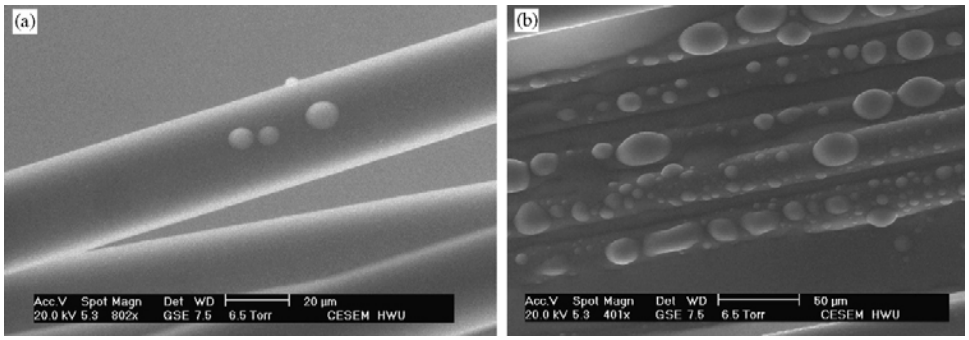

Figure 6. Wetting of needle punched polypropylene nonwoven by water.

The nonwoven industry is one of the fastest growing industries in the world [1]. Technological innovation and commercial development have been driving the industry into a sophisticated and diverse market with versatile products for a wide spectrum of applications in many industries, such as agricultural, automotive, building and construction, medical and hygiene, packaging, protective clothing, sportswear, transport, defense, leisure and safety.

One of the most important factors fuelling the growth of nonwovens is the development and application of man-made fibers, dominated by polyolefins [2].

For these increasing applications, nonwoven products are specially engineered to create the structure that gives the product its characteristic properties. The characterization of a nonwoven material under varying or dynamic conditions is of importance in understanding how the particular structure of the material is engineered, and, therefore, how it relates to the properties of the product.

Microscopy technology has provided the tools for the observation, analysis, and explanation of phenomena occurring at a micrometer scale of textile materials [3]. Scanning electron microscopes (SEMs) have long been important instruments in these studies. However, the high vacuum and the imaging process in SEMs impose special requirements for specimen preparation. Specimens that are not naturally conductive must be coated with a thin layer of a conductive material to bleed off any charge on the specimens imposed by the incident electron beam. One major disadvantage of the SEM is that it is normally not possible to examine wet specimens or dynamic processes of specimens in a wet state. Environmental scanning electron microscopy (ESEM) is a newer development in microscope technology, which is specifically suited to dynamic experimentation on the micron scale [4].

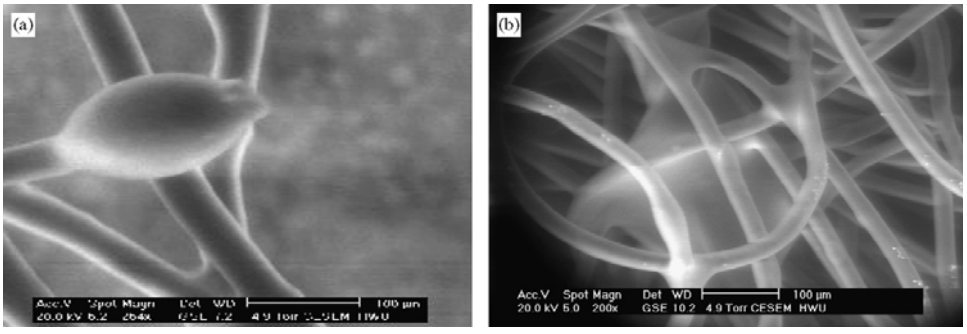

Figure 7. Oil adsorption of needle punched nonwoven.

The Philips XL30 ESEM was used for the dynamic experiments of water wetting, oil sorption and tensile deformation of polypropylene (PP) nonwovens in this study.

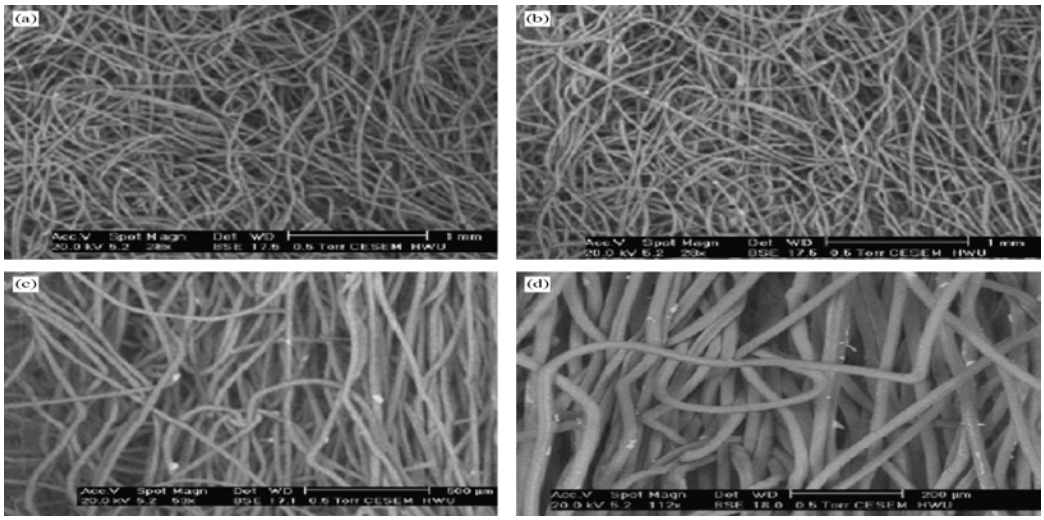

Figure 8. Loading deformation of needle punched nonwoven: (a) before tensile deformation; (b) deformation at 50% strain; (c) deformation at 100% strain and (d) deformation at 150% strain.

CONCLUSION

As a conclusion this study has explored the use of the ESEM for the examination and observation of PP nonwovens under varying conditions. The ability of the ESEM to follow dynamic events under a variety of conditions gives new insight into the dynamic wetting of water on fiber surface, the oil sorption in nonwovens and the tensile behavior of nonwoven materials. Direct observations of water droplets on the PP nonwovens reveal the high contact angles, indicating the hydrophobic properties of the fibers. The oil contact angles are lower than 201, indicating the affinity of PP fibers for oil. The ESEM studies also show the oil sorption on individual fibers, fiber intersections and fibrous pores in the PP nonwovens. The tensile testing in the ESEM gives some further evidence on the dynamic process of fiber orientation, rearrangement and breakdown in the PP nonwovens. ESEM provides a new and powerful approach to imaging of textile materials in connection with such applications as filtration, medical and hygiene, composites and biomedical products. The potential of use of ESEM in textile research and development is promising and significant.

REFERENCES

[1] X.Y. Wang ∗ , R.H. Gong, Z. Dong, I. Porte Textiles and Paper, School of Materials, the University of Manchester, P.O. Box 88, Sackville Street, Manchester, M60 1QD, UK Received 8 September 2005; received in revised form 23 May 2006; accepted 14 June 2006

[2] Myoung-Soo Won_, You-Seong KimDepartment of Civil Engineering, Chonbuk National University, 664-14 Deogjin-dong 1Ga, Deogjin-gu, Jeonju, Jeollabuk-do 561-756, South Korea Received 16 April 2006; received in revised form 29 September 2006; accepted 16 October 2006

[3] Amit Rawala,_, Rajesh Anandjiwalaa,b aCSIR, National Fiber, Textile and Clothing Centre, Port Elizabeth 6000, South Africa Department of Textile Science, Faculty of Science, Nelson Mandela Metropolitan University, Port Elizabeth, South Africa Received 10 February 2006; received in revised form 21 August 2006; accepted 27 August 2006

[4] Qufu Weia,b,_, Ya Liua, Xueqian Wangb, Fenglin Huanga aKey Laboratory of Science and Technology of Eco-textile Ministry of Education, Southern Yangtze University, Wuxi 214122, PR China bAnhui University of Technology and Science, Wuhu 241000, PR China Received 11 June 2006;

[5] Abdelmalek Bouazza_, Michelle Freund1, Hani Nahlawi Department of Civil Engineering, Building 60, Monash University, Melbourne, Vic. 3800, Australia Received 5 May 2006;

[6] Cho-Sen Wua,_, Yung-Shan Honga, Yun-Wei Yanb, Bow-Shung Changb aDepartment of Civil Engineering, Tamkang University, Tamsui, Taipei 25137, Taiwan bDepartment of Civil Engineering, Tamkang University, Taipei 106, Taiwan Received 18 September 2004; received in revised form 6 September 2005; accepted 7 September 2005

[7] Muhammet V. Akpinara,_, Craig H. Bensonb,1 aDepartment of Civil Engineering, Mustafa Kemal Universities, Tayfur Sokmen Campus, Hatay, Turkey bDepartment of Civil and Environmental Engineering, University of Wisconsin-Madison, Madison, WI 53706, USA

[8] G.L. Hebelera, J.D. Frosta,_, A.T. Myersb aSchool of Civil and Environmental Engineering, Georgia Institute of Technology, 790 Atlantic Drive, Atlanta, GA, USA bGeorgia Institute of Technology, Atlanta, GA, USA

[9] T. Iryoa, R. Kerry Roweb,*Department of Civil and Environmental Engineering, University of Western Ontario, London, Ont., Canada N6A 5B9 bGeoEngineering Centre of Queen's-RMC, Department of Civil Engineering, Queen's University, Ellis Hall, Kingston, Ont., Canada K7L 3N6 Received 10 March 2003; received in revised form 30 May 2003;

[10] D.T. Bergadoa,*, S. Youwaib, C.N. Haic, P. Voottipruexd a Geotechnical Engineering Program, School of Civil Engineering, Asian Institute of Technology, P.O. Box 4, Klong Luang, Pathumthani 12120, Thailand b School of Civil Engineering, Asian Institute of Technology, P.O. Box 4, Klong Luang, Pathumthani 12120, Thailand cThe Polytechnic University of HoChiMinh City, HoChiMinh City, Viet Nam d King Mongkut's Institute of Technology, North Bangkok, Piboonsongkram Rd., Bangsue District, Bangkok, Thailand Received 28 May 2000;

[11] J. Prabakara,*, R.S. Sridharb a*Regional Research laboratory* (*CSIR*), *Bhopal, India* b*Coimbatore Institute of Technology, Coimbatore, India* Received 21 July 2000; received in revised form 23 July 2001; accepted 9 January 2002

In: Monomers, Oligomers, Polymers, Composites… ISBN: 978-1-60456-877-6
Editors: R. A. Pethrick, G.E. Zaikov et al.

Chapter 15

SOME ASPECTS OF HEAT FLOW DURING DRYING OF POROUS STRUCTURES

A. K. Haghi*
University of Guilan, P. O.Box 3756, Rasht, Iran

ABSTRACT

In The first part of this chapter a detailed study on different aspects of heat flow in porous structures is presented. In the second part, a mathematical model was developed for optimization of heat and mass transfer in capillary porous media during drying process to predict the drying constants.

1.1. INTRODUCTION

For Heat flow analysis of wet porous materials, the liquid is water and the gas is air. Evaporation or condensation occurs at the interface between the water and air so that the air is mixed with water vapor. A flow of the mixture of air and vapor may be caused by external forces, for instance, by an imposed pressure difference. The vapor will also move relative to the gas by diffusion from regions where the partial pressure of the vapor is higher to those where it is lower.

Heat flow in porous media is the study of energy movement in the form of heat which occurs in many types of processes. The transfer of heat in porous media occurs from the high to the low temperature regions. Therefore a temperature gradient has to exist between the two regions for heat transfer to happen. It can be done by conduction (within one porous solid or between two porous solids in contact), by convection (between two fluids or a fluid and a porous solid in direct contact with the fluid), by radiation (transmission by electromagnetic waves through space) or by combination of the above three methods.

The general equation for heat transfer in porous media is:

* Haghi@Guilan.ac.ir

$$\begin{pmatrix}\text{rate of}\\ \text{heat in}\end{pmatrix} + \begin{pmatrix}\text{rate of generation}\\ \text{of heat}\end{pmatrix} = \begin{pmatrix}\text{rate of}\\ \text{heat out}\end{pmatrix} + \begin{pmatrix}\text{rate of accumulation}\\ \text{of heat}\end{pmatrix}$$

When a wet porous material is subjected to thermal drying two processes occur simultaneously, namely:

a. Transfer of heat to raise the wet porous media temperature and to evaporate the moisture content.
b. Transfer of mass in the form of internal moisture to the surface of the porous material and its subsequent evaporation.

The rate at which drying is accomplished is governed by the rate at which these two processes proceed. Heat is a form of energy that can across the boundary of a system. Heat can, therefore, be defined as "the form of energy that is transferred between a system and its surroundings as a result of a temperature difference". There can only be a transfer of energy across the boundary in the form of heat if there is a temperature difference between the system and its surroundings. Conversely, if the system and surroundings are at the same temperature there is no heat transfer across the boundary.

Strictly speaking, the term *"heat"* is a name given to the particular form of energy crossing the boundary. However, heat is more usually referred to in thermodynamics through the term "heat transfer", which is consistent with the ability of heat to raise or lower the energy within a system.

There are three modes of heat flow in porous media:

- convection
- conduction
- radiation

All three are different. Convection relies on movement of a fluid in porous material. Conduction relies on transfer of energy between molecules within a porous solid or fluid. Radiation is a form of electromagnetic energy transmission and is independent of any substance between the emitter and receiver of such energy. However, all three modes of heat flow rely on a temperature difference for the transfer of energy to take place.

The greater the temperature difference the more rapidly will the heat be transferred. Conversely, the lower the temperature difference, the slower will be the rate at which heat is transferred. When discussing the modes of heat transfer it is the rate of heat transfer Q that defines the characteristics rather than the quantity of heat.

As it was mentioned earlier, there are three modes of heat flow in porous structures, convection, conduction and radiation. Although two, or even all three, modes of heat flow may be combined in any particular thermodynamic situation, the three are quite different and will be introduced separately.

The coupled heat and liquid moisture transport of porous material has wide industrial applications. Heat transfer mechanisms in porous textiles include conduction by the solid material of fibers, conduction by intervening air, radiation, and convection. Meanwhile, liquid

and moisture transfer mechanisms include vapor diffusion in the void space and moisture sorption by the fiber, evaporation, and capillary effects. Water vapor moves through porous textiles as a result of water vapor concentration differences. Fibers absorb water vapor due to their internal chemical compositions and structures. The flow of liquid moisture through the textiles is caused by fiber-liquid molecular attraction at the surface of fiber materials, which is determined mainly by surface tension and effective capillary pore distribution and pathways. Evaporation and/or condensation take place, depending on the temperature and moisture distributions. The heat transfer process is coupled with the moisture transfer processes with phase changes such as moisture sorption/desorption and evaporation/condensation.

1.2. HEAT FLOW AND DRYING OF POROUS STRUCTURES

All three of the mechanisms by which heat is transferred- conduction, radiation and convection, may enter into drying. The relative importance of the mechanisms varies from one drying process to another and very often one mode of heat transfer predominates to such extent that it governs the overall process.

As an example, in air drying the rate of heat transfer is given by:

$$q = h_s A(T_a - T_s) \tag{1.1}$$

Where q is the heat transfer rate in Js^{-1}, h_s is the surface heat-transfer coefficient in $Jm^{-2}\ s^{-1}\ {}^oC^{-1}$, A is the area through which heat flow is taking place, m^{-2}, T_a is the air temperature and T_s is the temperature of the surface which is drying, ^oC.

To take another example, in a cylindrical dryer where moist material is spread over the surface of a heated cylinder, heat transfer occurs by conduction from the cylinder to the porous media, so that the equation is

$$q = UA(T_i - T_s) \tag{1.2}$$

Where U is the overall heat-transfer coefficient, T_i is the cylinder temperature (usually very close to that of the steam), Ts is the surface temperature of textile and A is the area of the drying surface on the cylinder. The value of U can be estimated from the conductivity of the cylinder material and of the layer of porous solid.

Mass transfer in the drying of a wet porous material will depend on two mechanisms: movement of moisture within the porous material which will be a function of the internal physical nature of the solid and its moisture content; and the movement of water vapour from the material surface as a result of water vapour from the material surface as a result of external conditions of temperature, air humidity and flow, area of exposed surface and supernatant pressure.

Some porous materials such as textiles exposed to a hot air stream may be cooled evaporatively by bleeding water through its surface. Water vapour may condense out of damp air onto cool surfaces. Heat will flow through an air-water mixture in these situations, but water vapour will diffuse or convect through air as well. This sort of transport of one

substance relative to another called mass transfer. The moisture content, *X*, is described as the ratio of the amount of water in the materials, m_{H2O} to the dry weight of material, $m_{material}$:

$$X = \frac{m_{H2O}}{m_{material}} \tag{1.3}$$

There are large differences in quality between different porous materials depending on structure and type of material. A porous material such as textiles can be hydrophilic or hydrophobic. The hydrophilic fibres can absorb water, while hydrophobic fibers do not. A textile that transports water through its porous structures without absorbing moisture is preferable to use as a first layer. Mass transfer during drying depends on the transport within the fiber and from the textile surface, as well as on how the textile absorbs water, all of which will affect the drying process .

As the critical moisture content or the falling drying rate period is reached, the drying rate is less affected by external factors such as air velocity. Instead, the internal factors due to moisture transport in the material will have a larger impact. Moisture is transported in textile during drying through

- capillary flow of unbound water
- movement of bound water and
- vapour transfer

Unbound water in a porous media such as textile will be transported primarily by capillary flow .

As water is transported out of the porous material, air will be replacing the water in the pores. This will leave isolated areas of moisture where the capillary flow continues .

Moisture in a porous structure can be transferred in liquid and gaseous phases. Several modes of moisture transport can be distinguished:

- transport by liquid diffusion
- transport by vapour diffusion
- transport by effusion (Knudsen-type diffusion)
- transport by thermodiffusion
- transport by capillary forces
- transport by osmotic pressure and
- transport due to pressure gradient.

1.3. CONVECTION HEAT FLOW IN POROUS MEDIA

A very common method of removing water from porous structures is convective drying. Concevtion is a mode of heat transfer that takes place as a result of motion within a fluid. If the fluid, starts at a constant temperature and the surface is suddenly increased in temperature to above that of the fluid, there will be convective heat transfer from the surface to the fluid as

a result of the temperature difference. Under these conditions the temperature difference causing the heat transfer can be defined as:

ΔT = surface temperature-mean fluid temperature

Using this definition of the temperature difference, the rate of heat transfer due to convection can be evaluated using Newton's law of cooling:

$$Q = h_c A \Delta T \tag{1.4}$$

where A is the heat transfer surface area and h_c is the coefficient of heat transfer from the surface to the fluid, referred to as the "convective heat transfer coefficient".

The units of the convective heat transfer coefficient can be determined from the units of other variables:

$$\begin{aligned} Q &= h_c A \Delta T \\ W &= (h_c) m^2 K \end{aligned} \tag{1.5}$$

so the units of h_c are $W / m^2 K$.

The relationships given in equations (1.4 and 1.5) are also true for the situation where a surface is being heated due to the fluid having higher temperature than the surface. However, in this case the direction of heat transfer is from the fluid to the surface and the temperature difference will now be

ΔT = mean fluid temperature-surface temperature

The relative temperatures of the surface and fluid determine the direction of heat transfer and the rate at which heat transfer take place.

As given in previous equations, the rate of heat transfer is not only determined by the temperature difference but also by the convective heat transfer coefficient h_c. This is not a constant but varies quite widely depending on the properties of the fluid and the behaviour of the flow. The value of h_c must depend on the thermal capacity of the fluid particle considered, i.e. mC_p for the particle. So the higher the density and C_p of the fluid the better the convective heat transfer.

Two common heat transfer fluids are air and water, due to their widespread availability. Water is approximately 800 times more dense than air and also has a higher value of C_p. If the argument given above is valid then water has a higher thermal capacity than air and should have a better convective heat transfer performance. This is borne out in practice because typical values of convective heat transfer coefficients are as follows:

Fluid	$h_c\left(W/m^2K\right)$
water	500-10000
air	5-100

The variation in the values reflects the variation in the behaviour of the flow, particularly the flow velocity, with the higher values of h_c resulting from higher flow velocities over the surface.

When a fluid is in forced or natural convective motion along a surface, the rate of heat transfer between the solid and the fluid is expressed by the following equation:

$$q = h.A\left(T_W - T_f\right) \tag{1.6}$$

The coefficient *h* is dependent on the system geometry, the fluid properties and velocity and the temperature gradient. Most of the resistance to heat transfer happens in the stationary layer of fluid present at the surface of the solid, therefore the coefficient *h* is often called film coefficient.

Correlations for predicting film coefficient *h* are semi empirical and use dimensionless numbers which describe the physical properties of the fluid, the type of flow, the temperature difference and the geometry of the system.

The Reynolds Number characterizes the flow properties (laminar or turbulent). *L* is the characteristic length: length for a plate, diameter for cylinder or sphere.

$$N_{\mathrm{Re}} = \frac{\rho L \nu}{\mu} \tag{1.7}$$

The Prandtl Number characterizes the physical properties of the fluid for the viscous layer near the wall.

$$N_{\mathrm{Pr}} = \frac{\mu c_p}{k} \tag{1.8}$$

The Nusselt Number relates the heat transfer coefficient *h* to the thermal conductivity *k* of the fluid.

$$N_{Nu} = \frac{hL}{k} \tag{1.9}$$

The Grashof Number characterizes the physical properties of the fluid for natural convection.

$$N_{Gr} = \frac{L^3 \Delta\rho g}{\rho\gamma^2} = \frac{L^3 \rho^2 g\beta\Delta T}{\mu^2} \tag{1.10}$$

1.4. CONDUCTION HEAT FLOW IN POROUS MATERIALS

If a fluid could be kept stationary there would be no convection taking place. However, it would still be possible to transfer heat by means of conduction. Conduction depends on the transfer of energy from one molecule to another within the heat transfer medium and, in this sense, thermal conduction is analogous to electrical conduction.

Conduction can occur within both porous solids and fluids. The rate of heat transfer depends on a physical property of the particular porous solid of fluid, termed its thermal conductivity k, and the temperature gradient across the porous medium. The thermal conductivity is defined as the measure of the rate of heat transfer across a unit width of porous material, for a unit cross-sectional area and for a unit difference in temperature.

From the definition of thermal conductivity k it can be shown that the rate of heat transfer is given by the relationship:

$$Q = \frac{kA\Delta T}{x} \tag{1.12}$$

where ΔT is the temperature difference $T_1 - T_2$, defined by the temperature on the either side of the porous solid. The units of thermal conductivity can be determined from the units of the other variables:

$$\begin{aligned} Q &= kA\Delta T / x \\ W &= (k)m^2 K / m \end{aligned} \tag{1.13}$$

so the unit of k are $W / m^2 K / m$, expressed as W/mK.

Fourier's Law can be integrated through a flat wall of constant cross section *A* for the case of steady-state heat transfer when the thermal conductivity of the wall *k* is constant.

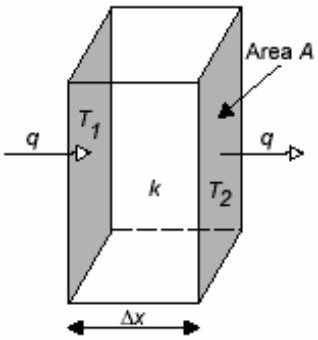

$$\frac{q}{A}\int_{x_1}^{x_2} dx = -k\int_{T_1}^{T_2} dT \rightarrow \frac{q}{A} = \frac{k}{\Delta x}\left(T_1 - T_2\right) \tag{1.14}$$

At any position x between x_1 and x_2, the temperature T varies linearly with the distance:

$$\frac{q}{A} = \frac{k}{x - x_1}\left(T_1 - T\right) \tag{1.15}$$

1.5. RADIATION HEAT FLOW IN POROUS SOLIDS

The third mode of heat flow, radiation, does not depend on any medium for its transmission. In fact, it takes place most freely when there is a perfect vacuum between the emitter and the receiver of such energy. This is proved daily by the transfer of energy from the sun to the earth across the intervening space.

Radiation is a form of electromagnetic energy transmission and takes place between all matters providing that it is at a temperature above absolute zero. Infra-red radiation form just part of the overall electromagnetic spectrum. Radiation is energy emitted by the electrons vibrating in the molecules at the surface of a porous body. The amount of energy that can be transferred depends on the absolute temperature of the porous body and the radiant properties of the surface.

A porous body that has a surface that will absorb all the radiant energy it receives is an ideal radiator, termed a "black body". Such a porous body will not only absorb radiation at a maximum level but will also emit radiation at a maximum level. However, in practice, porous bodies do not have the surface characteristics of a black body and will always absorb, or emit, radiant energy at a lower level than a black body.

It is possible to define how much of the radiant energy will be absorbed, or emitted, by a particular surface by the use of a correction factor, known as the "emissivity" and given the symbol ε. The emmisivity of a surface is the measure of the actual amount of radiant energy that can be absorbed, compared to a black body. Similarly, the emissivity defines the radiant energy emitted from a surface compared to a black body. A black body would, therefore, by definition, have an emissivity ε of 1.

Since World War II, there have been major developments in the use of microwaves for heating applications. After this time it was realized that microwaves had the potential to provide rapid, energy-efficient heating of materials. These main applications of microwave heating today include food processing, wood drying, plastic and rubber treating as well as curing and preheating of ceramics. Broadly speaking, microwave radiation is the term associated with any electromagnetic radiation in the microwave frequency range of 300 MHz-300 Ghz. Domestic and industrial microwave ovens generally operate at a frequency of 2.45 Ghz corresponding to a wavelength of 12.2 cm. However, not all materials can be heated rapidly by microwaves. Porous materials may be classified into three groups, *i.e.* conductors insulators and absorbers. Porous materials that absorb microwave radiation are called dielectrics, thus, microwave heating is also referred to as dielectric heating. Dielectrics have two important properties:

- They have very few charge carriers. When an external electric field is applied there is very little change carried through the material matrix.
- The molecules or atoms comprising the dielectric exhibit a dipole movement distance.

An example of this is the stereochemistry of covalent bonds in a water molecule, giving the water molecule a dipole movement. Water is the typical case of non-symmetric molecule. Dipoles may be a natural feature of the dielectric or they may be induced. Distortion of the electron cloud around non-polar molecules or atoms through the presence of an external electric field can induce a temporary dipole movement. This movement generates friction inside the dielectric and the energy is dissipated subsequently as heat.

The interaction of dielectric materials with electromagnetic radiation in the microwave range results in energy absorbance. The ability of a material to absorb energy while in a microwave cavity is related to the loss tangent of the material.

This depends on the relaxation times of the molecules in the material, which, in turn, depends on the nature of the functional groups and the volume of the molecule. Generally, the dielectric properties of a material are related to temperature, moisture content, density and material geometry.

An important characteristic of microwave heating is the phenomenon of “hot spot” formation, whereby regions of very high temperature form due to non-uniform heating. This thermal instability arises because of the non-linear dependence of the electromagnetic and thermal properties of material on temperature. The formation of standing waves within the microwave cavity results in some regions being exposed to higher energy than others. This result in an increased rate of heating in these higher energy areas due to the non-linear dependence. Cavity design is an important factor in the control, or the utilization of this “hot spots” phenomenon.

Microwave energy is extremely efficient in the selective heating of materials as no energy is wasted in “bulk heating” the sample. This is a clear advantage that microwave heating has over conventional methods. Microwave heating processes are currently undergoing investigation for application in a number of fields where the advantages of microwave energy may lead to significant savings in energy consumption, process time and environmental remediation.

Compared with conventional heating techniques, microwave heating has the following additional advantages:

- higher heating rates;
- no direct contact between the heating source and the heated material;
- selective heating may be achieved;
- greater control of the heating or drying process;
- reduced equipment size and waste.

As mentioned earlier, radiation is a term applied to many processes which involve energy transfer by electromagnetic wave (x rays, light, gamma rays ...). It obeys the same laws as light, travels in straight lines and can be transmitted through space and vacuum. It is an important mode of heat transfer encountered where large temperature difference occurs between two surfaces such as in furnaces, radiant driers and baking ovens.

The thermal energy of the hot source is converted into the energy of electromagnetic waves. These waves travel through space into straight lines and strike a cold surface. The waves that strike the cold body are absorbed by that body and converted back to thermal energy or heat. When thermal radiations falls upon a body, part is absorbed by the body in the form of heat, part is reflected back into space and in some case part can be transmitted through the body.

The basic equation for heat transfer by radiation from a body at temperature T is:

$$q = A\varepsilon\sigma T^4 \tag{1.16}$$

where ϵ is the emissivity of the body. ϵ = 1 for a perfect black body while real bodies which are gray bodies have an ϵ < 1

1.6. Porosity and Pore Size Distribution in a Body

Porosity refers to volume fraction of void spaces. This void space can be actual space filled with air or space filled with both water and air. Many different definitions of porosity are possible. For non-hygroscopic materials, porosity does not change with change in moisture content. For hygroscopic materials, porosity changes with moisture content. However, such changes during processing are complex due to consideration of bound water and are typically not included in computations.

The distinction between porous and capillary-porous is based on the presence and size of the pores. Porous materials are sometimes defined as those having pore diameter greater than or equal to 10^{-7} m and capillary-porous as one having diameter less than 10^{-7} m. Porous and capillary porous materials were defined as those having a clearly recognizable pore space.

In non-hygroscopic materials, the pore space is filled with liquid if the material is completely saturated and with air if it is completely dry. The amount of physically bound water is negligible. Such a material does not shrink during heating. In non-hygroscopic materials, vapour pressure is a function of temperature only. Examples of non-hygroscopic capillary-porous materials are sand, polymer particles and some ceramics. Transport materials in non-hygroscopic materials do not cause any additional complications as in hygroscopic materials.

In hygroscopic materials, there is large amount of physically bound water and the material often shrinks during heating. In hygroscopic materials there is a level of moisture saturation below which the internal vapour pressure is a function of saturation and temperature. These relationships are called equilibrium moisture isotherms. Above this moisture saturation, the vapour pressure is a function of temperature only and independent of the moisture level. Thus, above certain moisture level, all materials behave non-hygroscopic.

Transport of water in hygroscopic materials can be complex. The unbound water can be in funicular and pendular states. This bound water is removed by progressive vaporization below the surface of the solid, which is accompanied by diffusion of water vapour through the solid.

Examples of porous materials are to be found in everyday life. Soil, porous or fissured rocks, ceramics, fibrous aggregates, sand filters, snow layers and a piece of sugar or bread are

but just a few. All of these materials have properties in common that intuitively lead us to classify them into a single denomination: *porous media*.

Indeed, one recognizes a common feature to all these examples. All are described as "solids" with "holes", i.e. presenting *connected void spaces*, distributed - randomly or quite homogeneously - within a *solid matrix*. Fluid flows can occur within the porous medium, so that we add one essential feature: this *void space* consists of a complex tridimensional network of *interconnected* small empty volumes called "*pores*", with several continuous paths linking up the porous matrix spatial extension, to enable flow across the sample.

If we consider a porous medium that is not consolidated, it is possible to derive the *particle-size distribution* of the constitutive solid grains. The problem is obvious when dealing with spherical shaped particles, but raises the question of what is meant by particle size in the case of an irregular shaped particle. In both cases, a first intuitive approach is to start with a *sieve analysis*. It consists to sort the constitutive solid particles among various sieves, each one having a calibrated mesh size. The most common type of sieve is a woven cloth of stainless steel or other metal, with wire diameter and tightness of weave controlled to produced roughly rectangular openings of known, uniform size. By shaking adequately the raw granular material, the solid grains are progressively falling through the stacked sieves of decreasing mesh sizes, i.e. a *sieve column*. We finally get separation of the grains as function of their *particle- size* distribution that is also denoted by the porous medium *granulometry*. This method can be implemented for dry granular samples. The *sieve analysis* is a very simple and inexpensive separation method, but the reported granulometry depends very much on the shape of the particles and the duration of the laboratory test, since the sieve will let in theory pass any particle with a smallest cross-section smaller than the nominal mesh opening. For example, one gets very different figure while comparing long thin particles to spherical particles of the same weight.

The definition of a porous medium can be based on the objective of describing flow in porous media. A porous medium is a heterogeneous system consisting of a rigid and stationary solid matrix and fluid filled voids. The solid matrix or phase is always continuous and fully connected. A phase is considered a homogeneous portion of a system, which is separated from other such portions by a definitive boundary, called an interface. The size of the voids or pores is large enough such that the contained fluids can be treated as a continuum. On the other hand, they are small enough that the interface between different fluids is not significantly affected by gravity.

The topology of the solid phase determines if the porous medium is permeable, i.e. if fluid can flow through it, and the geometry determines the resistance to flown and therefore the permeability. The most important influence of the geometry on the permeability is through the interfacial or surface area between the solid phase and the fluid phase. The topology and geometry also determine if a porous medium is isotropic, i.e. all parameters are independent of orientation or anisotropic if the parameters depend on orientation. In multi-phase flow the geometry and surface characteristics of the solid phase determine the fluid distribution in the pores, as does the interaction between the fluids. A porous medium is homogeneous if its average properties are independent of location, and heterogeneous if they depend on location. An example of a porous medium is sand. Sand is an unconsolidated porous medium, and the grains have predominantly point contact. Because of the irregular and angular nature of sand grains, many wedge-like crevices are present. An important quantitative aspect is the surface area of the sand grains exposed to the fluid. It determines the

amount of water which can be held by capillary forces against the action of gravity and influences the degree of permeability.

The fluid phase occupying the voids can be heterogeneous in itself, consisting of any number of miscible or immiscible fluids. If a specific fluid phase is connected, continuous flow is possible. If the specific fluid phase is not connected, it can still have bulk movement in ganglia or drops. For single-phase flow the movement of a Newtonian fluid is described. For two-phase immiscible flow, a viscous Newtonian wetting liquid together with a non-viscous gas are described. In practice these would be water and air.

1.7. PORE-SIZE DISTRIBUTION IN POROUS STRUCTURE

A detailed description of the complex tri-dimensional network of pores is obviously impossible to derive. For consolidated porous media, the determination of a *pore-size distribution* is nevertheless useful. For those particular media, it is indeed impossible to handle any particle-size distribution analysis.

One approach to define a *pore size* is in the following way: the *pore diameter* δ at a given point within the pore space is the diameter of the largest sphere that contains this point, while still remaining entirely within the pore space. To each point of the *pore space* such a "diameter" can be attached rigorously, and the *pore-size distribution* can be derived by introducing the *pore-size density function* $\theta(\delta)$ defined as the fraction of the total void space that has a pore diameter comprised between δ and $\delta + d\delta$. This distribution is normalized by the relation:

$$\int_0^\infty \theta(\delta) d\delta = 1 \tag{1.17}$$

A *porous structure* should be:

- A material medium made of heterogeneous or multiphase matter. At least one of the considered phases is not solid. The solid phase is usually called the *solid matrix*. The space within the porous medium domain that is not part of the *solid matrix* is named *void space* or *pore space*. It is filled by gaseous and/or liquid phases.
- The solid phase should be distributed throughout the porous medium to draw a network of pores, whose characteristic size can vary greatly. Some of the pores comprising the void space must enable the flow across the solid matrix, so that they should then be interconnected.
- The interconnected pore space is often denoted as the *effective pore space*, while unconnected pores may be considered from the hydrodynamic point of view as part of the solid matrix, since those pores are ineffective as far as flow through the porous medium is concerned. They are *dead-end pores* or *blind pores*, that contain stagnant fluid and no flow occurs through them.

A porous material is a set of pores embedded in a matrix of mostly solid material. The pores are the voids in the material itself. Pores can be isolated or interconnected. Furthermore, a pore can contain a fluid or a vapor, but it can also be empty. If the pore is completely filled with the fluid, it will be called saturated and if it is partially filled, it will be called non-saturated. So the porous material is primarily characterized by the content of its voids and not by the properties of the material itself. Figure 1 gives a sketch of a porous material.

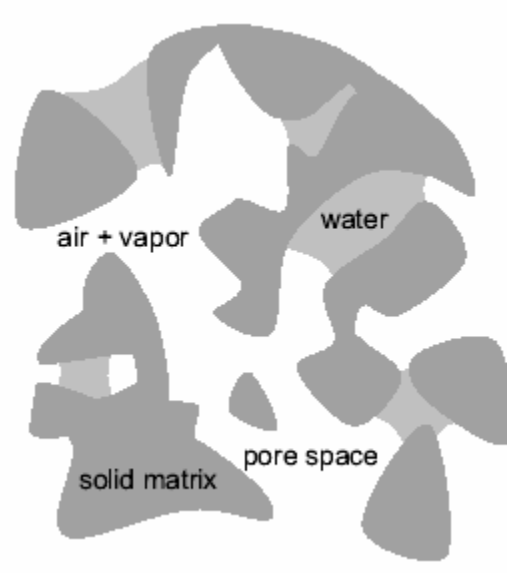

Figure 1.1. A 2D sketch of a non-saturated porous material.

If the pores are not interconnected very well, the relaxation-time distribution of an NMR(Nuclear Magnetic Resonance) spin-echo measurement can be interpreted in terms of a pore-size distribution (PSD). For magnetically doped materials like clay and .red-clay this so-called relaxometry technique gives a pore-size distribution between 100 nm and 100 μm, which is also the range of the majority of the pores in these materials. NMR (Nuclear Magnetic Resonance) can be used for spectroscopy, because different nuclei resonate at different frequencies and can therefore be distinguished from each other. Not only nuclei, but also different isotopes can be distinguished. Since also the surrounding of the nucleus has an effect on the exact resonance frequency, NMR spectroscopy is also used to distinguish specific molecules. By manipulating the spatial dependence of the magnetic field strength and the frequency of the RF excitation, the NMR sensitive region can be varied. This enables a noninvasive measurement of the spatial distribution of a certain nucleus and is called NMR Imaging (MRI).

In many NMR experiments it was noticed that liquids confined in porous materials exhibit properties that are very different from those of the bulk fluid. The so-called longitudinal ($T1$) and transverse ($T2$) relaxation time of bulk water, *e.g.*, are on the order of seconds, whereas for water in a porous material these times can be on the order of milliseconds. The measurement of $T1$ and $T2$ in an NMR experiment is often called NMR relaxometry. The transverse relaxation time is more sensitive to local magnetic field gradients inside the porous material than the longitudinal relaxation time. This sensitivity can be used

to measure the self-di.usion coe.cient of the liquid. The interpretation of the measured self-diffusion coefficient of a confined liquid is often called NMR diffusometry.

Nuclear Magnetic Resonance is based on the following principle. When a nucleus is placed in a static magnetic field, the nuclear spin _*I* will start to presses around this field, since the magnetic moment $\overline{\mu}$ of the nucleus is related to the nuclear spin $\bar{I}$ (figure 2).

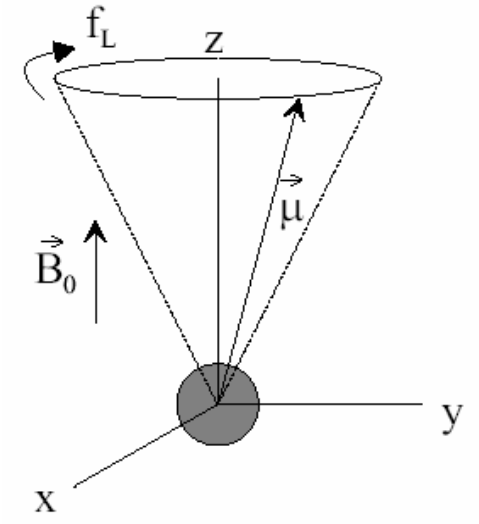

Figure 1.2. Larmor precession of a nuclear magnetic moment in a magnetic field.

The frequency of this precession motion is called the Larmor frequency:

$$f_L = \frac{\gamma}{2\pi} B_0 \tag{1.18}$$

where B_0 is the magnitude of the static magnetic field, which is usually taken aligned with the *z*-axis, f_L is the Larmor frequency and γ is the gyromagnetic ratio of the nucleus.

The NMR resonance condition (Eq. 1.18) states that the Larmor frequency depends linearly on the magnetic field. Normally one starts to assume that the magnetic field in the porous material is equal to the magnetic field generated by the experimental setup. This can be either the magnetic field emerging from a permanent magnet, an electromagnet, or a superconducting magnet. Frequently, an extra magnetic field gradient is added to the main magnetic field. This magnetic field gradient is used to discriminate spins at a certain position from spins at other positions. It is the basic principle of NMR Imaging (MRI). However, the magnetic field inside the porous sample can deviate largely from the magnetic field applied externally.

Because the magnetic susceptibility of the porous material differs from that of the surrounding air, the magnetic field inside the porous sample will deviate from the magnetic field that is present in the sample chamber or insert. Apart from this, the magnetic field in the pores of the material may differ from that in the bulk matrix. Consider two media with a different susceptibility. If the magnetic susceptibility of the sphere is larger (figure 3 on the

left) than that of the environment, the magnetic field inside this sphere is larger than the external magnetic field and the sphere is called paramagnetic. If, on the other hand, the susceptibility of the sphere is smaller (figure 3 on the right) than that of the environment, the magnetic field inside the sphere is smaller than the external magnetic field and the sphere is called diamagnetic.

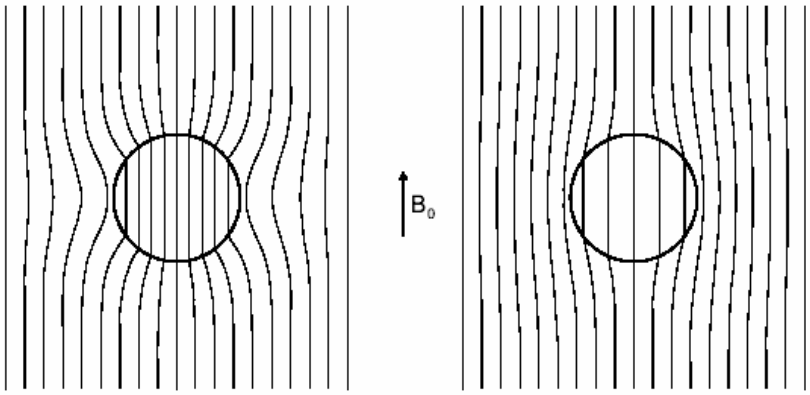

Figure 1.3. Disturbance of homogeneous magnetic field B_0 by an object with different susceptibility. Plotted are the magnetic field lines. On the left: a paramagnetic sphere; on the right: a diamagnetic sphere.

The amount of water in a porous body such as the textiles at the EMC is defined as bound water and it is absorbed by the textile fibers. When the textile is unable to absorb more water, all excess water is defined as unbound moisture. The unbound moisture is often found as a continuous liquid within the porous material.

Drying of porous media is accomplished by vaporizing the water and to do this the latent heat of vaporization must be supplied. There are, thus, two important process-controlling factors that enter into the process of drying:

(a) transfer of heat to provide the necessary latent heat of vaporization,
(b) movement of water or water vapour through textiles and then away from it to effect separation of water.

1.8. BASIC FLOW RELATIONS IN POROUS BODY

The motion of a fluid is described by the basic hydrodynamic equations, the continuity equation

$$\partial_t \rho + \nabla.(\rho u) = 0 \tag{1.19}$$

which expresses the conservation of mass, and the momentum equation

$$\partial_t(\rho u) + \nabla.(\rho u) = -\nabla p + \nabla.\tau + \rho g \tag{1.20}$$

which expresses the conservation of momentum. Here ρ is the fluid density, u the fluid velocity, p the hydrostatic pressure, τ the fluid stress tensor, and g the acceleration due to external forces including e.g. the effect of gravity on the fluid.

The equation for energy conservation can be written as

$$\rho \frac{d\hat{u}}{dt} + p(\nabla.u) = \nabla.(k\nabla T) + \Phi \tag{1.21}$$

where T is temperature, k the coefficient of thermal conductivity of the fluid, Φ the viscous dissipation function, and the density of thermal energy $\hat{u} = \hat{u}(p,T)$ is often approximated such that $d\hat{u} \approx c_v dT$, where c_v is the specific heat.

At low Reynolds numbers, the most important relation describing fluid transport through porous media is Darcy's law

$$q = -\frac{k}{\mu}\nabla p \tag{1.22}$$

where q is the volumetric fluid flow through the (homogeneous) medium and k is the permeability coefficient that measures the conductivity to fluid flow of the porous material.

1.9. TRANSPORT MECHANISMS IN POROUS MEDIA

The study of flow systems which compose of a porous medium and a homogenous fluid has attracted much attention since they occur in a wide range of the industrial and environmental applications. Examples of practical applications are: flow past porous scaffolds in bioreactors, drying process, electronic cooling, ceramic processing, and overland flow during rainfall, and ground-water pollution.

In the single-domain approach, the composite region is considered as a continuum and one set of general governing equations is applied for the whole domain. The explicit formulation of boundary conditions is avoided at the interface and the transitions of the properties between the fluid and porous medium are achieved by certain artifacts. Although this method is relatively easier to implement, the flow behavior at the interface may not be simulated properly, depending on how the code is structured.

In the two-domain approach, two sets of governing equations are applied to describe the flow in the two regions and additional boundary conditions are applied at the interface to close the two set of equations. This method is more reliable since it tries to simulate the flow behavior at the interface. Hence, in the present study, the two-domain approach, and the implementation of the interface boundary conditions, will be considered.

Fluid flow in a porous medium is a common phenomenon in nature, and in many fields of science and engineering. Important everyday flow phenomena include transport of water in

living plants and trees, and fertilizers or wastes in soil. Moreover, there is a wide variety of technical processes that involve fluid dynamics in various branches of process industry. The importance of improving our understanding of such processes arises from the high amount of energy consumed by them. In oil recovery, for example, a typical problem is the amount of unrecovered oil left in oil reservoirs by traditional recovery techniques. In many cases the porous structure of the medium and the related fluid flow are very complex, and detailed studies of these flows pose demanding tasks even in the case of stationary single-fluid flow. In experimental and theoretical work on fluid flow in porous materials it is typically relevant to find correlations between material characteristics, such as porosity and specific surface area, and flow properties. The most important phenomenological law governing the flow properties, first discovered by Darcy, defines the permeability as conductivity to fluid flow of the porous material. Permeability is given by the coefficient of linear response of the fluid to a non-zero pressure gradient in terms of the flux induced.

Some of the material properties that affect the permeability, e.g. tortuosity, are difficult to determine accurately with experimental techniques, which have been, for a long time, the only practical way to study many fluid-dynamical problems. Improvement of computers and the subsequent development of methods of computational fluid dynamics (CFD) have gradually made it possible to directly solve many complex fluid-dynamical problems. Flow is determined by its velocity and pressure fields, and the CFD methods typically solve these in a discrete computational grid generated in the fluid phases of the system. Traditionally CFD has concentrated on finding solution to differential continuum equations that govern the fluid flow. The results of many conventional methods are sensitive to grid generation which most often can be the main effort in the application. A successfully generated grid is typically an irregular mesh including knotty details that follow the expected streamlines.

Transport in a porous media can be due to several different mechanisms. Three of these mechanisms are often considered most dominant: molecular diffusion, capillary diffusion, and convection (*Darcy flow*).

The *Darcy law* has been derived as follows: we consider a macroscopic porous medium which has a cross section *A* and overall length *L*, and we impose an oriented fluid flow rate $\vec{Q}$, to flow through it .When a steady state is reached, the induced hydrostatic pressure gradient $\vec{\nabla} p$ is related to $\vec{Q}$ by the vectorial formula :

Fluid dynamics (also called fluid mechanics) is the study of moving (deformable) matter, and includes liquids and gases, plasmas and, to some extent, plastic solids. From a 'fluid-mechanical' point of view, matter can, in a broad sense, be considered to consist of fluid and solid, in a one-fluid system the difference between these two states being that a solid can resist shear stress by a static deformation, but a fluid can not . Notice also that thermodynamically a distinction between the gas and liquid states of matter cannot be made if temperature is above that of the so-called critical point, and below that temperature the only essential differences between these two phases are their differing equilibrium densities and compressibility.

$$\frac{\vec{Q}}{A} = \frac{\overline{\overline{K}}}{\mu_f}.\left(\vec{\nabla} p - \rho_f .\vec{g}\right) \Leftrightarrow \vec{v}_m = \frac{\overline{\overline{K}}}{\mu_f}.\left(\frac{\vec{\Delta} p}{L} - \rho_f .\vec{g}\right) \tag{1.23}$$

where $\vec{g}$ is the acceleration of the gravity field, ρ_f and μ_f are respectively the *specific mass* and the *dynamic viscosity* of fluid, $\vec{v}_m$ the *filtration velocity* over the cross section *A*. Formula (1.23) defines a second order symmetrical tensor $\overline{K}$, the *permeability*. It takes into account the macroscopic influence of the porous structure from the "resistance to the flow" point of view. The more permeable a porous medium is, the less it will resist to an imposed flow. The *permeability* is an intrinsic property of the porous matrix, based only on geometrical considerations, and is expressed in [m^2]. The tensorial character of $\overline{K}$ reflects the porous matrix *anisotropy*.

At the surface of the textile, two processes occur simultaneously in drying: heat transfer from the air to the drying surface and mass transfer from the drying surface to the surrounding air. The energy transfer between a surface and a fluid moving over the surface is traditionally described by convection. The unbound moisture on the surface of the material is first vaporised during the constant drying rate period.

Heat transfer by convection is described as

$$\frac{dQ}{dt} = \bar{h}A\left(T_A - T_S\right) \tag{1.24}$$

where *dQ/dt* is the rate of heat transfer, $h[W/m^2K]$ is the average heat transfer coefficient for the entire surface, *A*. T_S is the temperature of the material surface and T_A is the air temperature. The temperature on the surface is close to the wet bulb temperature of the air when unbound water is evaporated .

A similar equation describes the convective mass transfer. The total molar transfer rate of water vapour from a surface, dN_v / dt [kmol/s], is determined by

$$\frac{dN_v}{dt} = \bar{h}_m A\left(C_{v,A} - C_{v,S}\right) \tag{1.25}$$

where $\bar{h}_m$ [m/s] is the average convection mass transfer coefficient for the entire surface, $C_{v,A}$ is the molar concentration of water vapour in the surrounding air and $C_{v,S}$ is the molar concentration on the surface of the solid with the units of [kmol/m3]. During the constant drying rate period the drying rate is controlled by the heat and/or mass transfer coefficients, the area exposed to the drying medium, and the difference in temperature and relative humidity between the drying air and the wet surface of the material (Bejan *et al*. 2004).

The average convection coefficients depend on the surface geometry of the material and the flow conditions. The heat transfer coefficient, *h* , can be determined by the average Nusselt number, $\overline{N}u$:

$$\overline{N}u = \frac{\bar{h}L}{k_A} = f\left(\mathrm{Re}, \mathrm{Pr}\right) \tag{1.26}$$

where k_A is the heat conductivity for the air and *L* is the characteristic length ofthe surface of interest. $\overline{Nu}$ shows the ratio of the heat transfer that depends on convection to the heat transfer that depends on conduction in the boundary layer. The Nusselt number is a function of the Reynold number,*Re*, and the Prantdl- number,*Pr*. *Pr* is the relation between the thickness of the thermal and the velocity boundary layers. If *Pr*=1, the thickness of the thermal and velocity boundary layers are equal. For air *Pr*=0.7. To determine the mass transfer coefficient, $\overline{h}_m$, the average Sherwood-number, $\overline{Sh}$ is used:

$$\overline{Sh} = \frac{\overline{h}_m L}{D_{AS}} = f(\mathrm{Re}, Sc) \tag{1.27}$$

where D_{AS} is the diffusion coefficient. $\overline{Sh}$ is a function of the Reynold number, *Re*, and the Schmidt number, *Sc*, which is the relation between the thickness of the concentration and the velocity boundary layers.

1.10. MOLECULAR DIFFUSION IN POROUS STRUCTURES

Water vapour in the porous media can move by molecular or Fickian diffusion if the pores are large enough. Molecular diffusion is described by Fick's law

$$J = -D\frac{\partial c}{\partial x} \tag{1.28}$$

Where D is the molecular diffusivity.

Flow in porous media plays an important role in many areas of science and engineering. Examples of the application of porous media flow phenomena are as diverse as flow in human lungs or flow due to solidification in the mushy zone of liquid metals.

Flow in porous media is difficult to be accurately modeled quantitatively. Richards equation can give good results, but needs constitutive relations. These are usually empirically based and require extensive calibration. The parameters needed in the calibration are amongst others: capillary pressure and pressure gradient, volumetric flow, liquid content, irreducible liquid content, and temperature. In practice it is usually too demanding to measure all these parameters.

The description of the behavior of fluids in porous media is based on knowledge gained in studying these fluids in pure form. Flow and transport phenomena are described analogous to the movement of pure fluids without the presence of a porous medium. The presence of a permeable solid influences these phenomena significantly. The individual description of the movement of the fluid phases and their interaction with the solid phase is modeled by an up-scaled porous media flow equation. The concept of up-scaling from small to large scales is widely used in physics. Statistical physics translates the description of individual molecules

into a continuum description of different phases, which in turn is translated by volume averaging into a continuum porous medium description.

2. CASE STUDY

A mathematical model was developed for optimization of heat and mass transfer in capillary porous media during drying process to predict the drying constants. The modeling equations verified the experimental results and proved to be an important tool in predicting the drying rate under different drying conditions. The importance of heat and mass transfer in capillary porous materials like wood has increased in the last few decades due to its wide industrial as well as research applications. In order to reduce moisture content in woods to a level low enough, to prevent undesirable biochemical reactions and microbiological growth, prolonged drying time and high temperature must often be used. In practice, several different techniques are used; natural drying, vacuum drying, convectional convective drying, high temperature convective drying, and more recently microwave drying [1].

Several physical mechanisms contribute to moisture migration during the process. For a porous solid matrix, with free water, bound water, vapor, and air, moisture transport through the matrix can be in the form of either diffusion or capillary flow driven by individual or combined effects of moisture, temperature and pressure gradients. The predominant mechanisms that control moisture transfer depend on the hygroscopic nature and properties of the materials, as well as the heating conditions and the way heat is supplied. In this regard, there is a need to assess the effects of the heat and mass transfer within the wood on the transfer in the fluid adjacent to it.

There are three stages of drying: In the first stage when both surface and core MC are greater than the FSP. Moisture movement is by capillary flow. Drying rate is evaporation controlled. In the second stage when surface MC is less than the FSP and core MC is greater than the FSP. Drying is by capillary flow in the core and by bound water diffusion near the surface as fiber saturation line recedes into wood, resistance to drying increases. Drying rate is controlled by bound water diffusion and finally in the third stage when both surface and core MC is less than the FSP. Drying is entirely by diffusion. As the MC gradient between surface and core becomes less, resistance to drying increases and drying rate decreases.

For wood, model developments have been based on either a mechanistic approach with the transfer phenomena derived from Fick’s and Fourier’s laws, or on the principles of thermodynamics and entropy production. These models may be divided into three categories: (a) diffusion models [2], (b) models based on transport properties [3,4] and (c) models based on both the transport properties and the physiological properties of wood related to drying [5,6].

Drying adds value to timber but also costs money. Working out the complete cost of drying is a complex process. Timber drying is a critical and costly part of timber processing. Comparing the cost and effectiveness of drying systems and technology is an important exercise, before drying systems are commissioned or are upgraded. Reduction in drying time and energy consumption offers the wood industries a great potential for economic benefit. But the reduction in drying time often results in an increase in drying related defects such as checks, splits and warp.

In previous work drying curves were fitted to four drying models and the goodness of fit of each model (Correlation Coefficient and Standard Error) was evaluated [7]. The main aim of this work is to find out a model for drying time and to predict the required time for drying samples to desired moisture content. In the second part the forecast time is compared with the theoretical approach. The predicted values by the theoretical model are compared with experimental data taken under actual drying conditions to demonstrate the efficiency of the predictive model.

A software tool "Trend Analysis" for analysis the time series was applied. Trend analysis fits a general trend model to time series data and provides forecasts. S-curve is best fitted to our drying case. The S-curve model fits the Pearl-Reed logistic trend model. This accounts for the case where the series follows an S-shaped curve. The model is:

$$MC = \frac{10^{a}}{b_0 + b_1 b_2^{t}} \tag{2.1}$$

This tool is useful when we have dried the wood to moisture content not near to 30% and then predict the time needed to dry it completely.

Minitab computes three measures of accuracy of the fitted model: MAPE, MAD, and MSD for each of the simple forecasting and smoothing methods. For all three measures, the smaller the value, the better the fit of the model. These statistics are used to compare the fits of the different methods.

Mean Absolute Deviation (MAD) measures the accuracy of fitted time series values. It expresses accuracy in the same units as the data, which helps conceptualize the amount of error:

$$MAD = \frac{\sum_{t=1}^{n} \left| y_t - \hat{y}_t \right|}{n} \tag{2.2}$$

Where y_t equals the actual value at time $\hat{y}_t$ equals the fitted value, and n equals the number of observations.

Mean Absolute Percentage Error (MAPE) measures the accuracy of fitted time series values. It expresses accuracy as a percentage.

$$MAPE = \frac{\sum \left| \frac{\left(y_t - \hat{y}_t \right)}{y_t} \right|}{n} \times 100 \quad \left(y_t \neq 0 \right) \tag{2.3}$$

Where y_t equals the actual value at time $\hat{y}_t$ equals the fitted value, and n equals the number of observations.

MSD stands for Mean Squared Deviation. MSD is always computed using the same denominator, n, regardless of the model, so we can compare MSD values across models. MSD is a more sensitive measure of an unusually large forecast error than MAD.

$$MSD = \frac{\sum_{t=1}^{n} \left| y_t - \hat{y}_t \right|^2}{n} \tag{2.4}$$

Where y_t equals the actual value, t equals the forecast value, and n equals the number of forecasts.

2.1. GOVERNING EQUATIONS

Heat and mass transfer in a body take place simultaneously during the drying process. The time required to go from an initial moisture content, U_0, to a certain value $\overline{U}$ is given in[8]:

$$t = \frac{1.6 \times 10^{-4} S_x^2 S_y^2}{\left(\mu_{x1}^2 D_x S_y^2 + \mu_{y1}^2 D_y S_x^2 \right)} Log\left(\Gamma_{x1} \Gamma_{y1} \left(\frac{U_0 - U_{eq}}{\overline{U} - U_{eq}} \right) \right) \tag{2.5}$$

μ_{l1}^2 can be defined as:

$$\mu_{l1}^2 = \frac{1}{\frac{4}{\pi^2} + \frac{1}{B_l}} \tag{2.6}$$

Where B_l is the dimensionless constant called the "bio-criterion "of the sample:

$$B_l = \frac{\alpha_l R_l}{D_l} \tag{2.7}$$

Where R_l is half of the length of the rod, l is any of the two coordinates x,y, $S_x \times S_y$ is the width and thickness of sample, α_l is the coefficient of moisture exchange(m/s), D_l is the moisture diffusion coefficient(m^2 /s) which can vary in each of the different directions for the wood sample.

The value Γ_{l1} is determined as:

$$\Gamma_{l1} = \frac{2B_l^2}{\mu_{l1}^2\left(B_l^2 + B_l + \mu_{l1}^2\right)} \tag{2.8}$$

and an average dimensionless moisture content $\overline{E}_{\Sigma}$ is:

$$\overline{E}_{\Sigma} = \frac{\overline{U} - U_{eq}}{U_0 - U_{eq}} \tag{2.9}$$

U_{eq} is the equilibrium moisture content of the wood.

Another theoretical approach is presented by [9]:

$$t = \frac{65S^2}{\overline{D}10^6}\left(1 + \frac{\pi^2 D}{2\alpha s}\right)\log\frac{U_0 - U_{eq}}{\overline{U} - U_{eq}} \tag{2.10}$$

Where $\overline{D}$ is the average diffusion coefficient and $\overline{S}$ is the average length of the dimensions of specimens.

2.2. EXPERIMENTAL

Experimental material was obtained from two types of wood species, Guilan spruce and pine. The wood specimens were selected from Guilan region which is located in the north of Iran. The experiments were performed in a programmable domestic microwave drying system (Deawoo, KOC-1B4k) with a maximum power output of 1000 W at 2450MHz. Samples were dried in four methods: convection drying (150°C), microwave drying (270 W), infrared drying (100% power) and combination of microwave and convection drying. The dryer was run without the sample placed in, for about 30 min to set the desired drying conditions before each drying experiment. Throughout the experimental run the sample weights were continuously recorded at predetermined time intervals until wood reached to 30% of its moisture content.

2.3. RESULTS AND DISCUSSION

Figure 1-8 show the graphs moisture content variation against drying time, the model and the forecasted time for the four methods of drying on pine and Guilan spruce. Drying time is estimated to a moisture content of 14%. Results are relatively in a good agreement with drying curves. Just in some cases in heating up period this model didn't fit the experimental data closely. Heat is transferred by convection from heated air to the product to raise the temperatures of both the solid and moisture that is present. Moisture transfer occurs as the moisture travels to the evaporative surface of the product and then into the circulating air as water vapor. The heat and moisture transfer rates are therefore related to the velocity and

temperature of the circulating drying air. Moreover, the momentum transfer may take place simultaneously coupled with heat and moisture transfer. Convective drying at intermediate temperatures has proved to be very effective from the economical point of view, thanks to the short drying time, the reduced sizes of the kilns, and the better control of the energy consumption and the possibility of a good integration in the production line.

Infrared energy is transferred from the heating element to the product surface without heating the surrounding air. When infrared radiation is used to heat or dry moist materials, the radiation impinges the exposed material, penetrates it and the energy of radiation converts into heat. Since the material is heated intensely, the temperature gradient in the material reduces within a short period the depth of penetration of radiation depends upon the property of the material and wavelength of radiation. Further by application of intermittent radiation, wherein the period of heating the material is followed by cooling, intense displacement of moisture from core towards surface can be achieved.

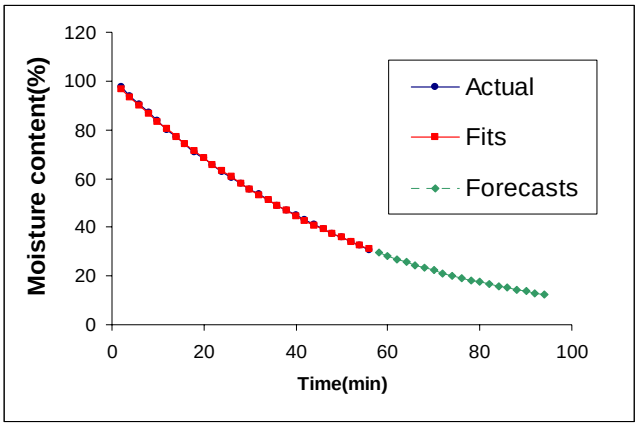

Figure 2.1. Moisture content vs. time for pine, (Convection drying).

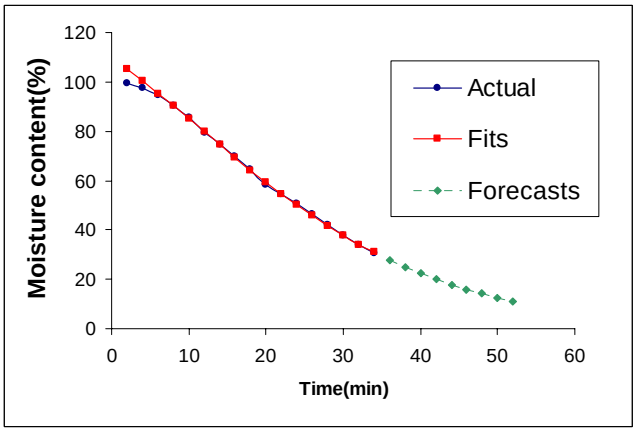

Figure 2.2. Moisture content vs. time for pine, (Infrared drying).

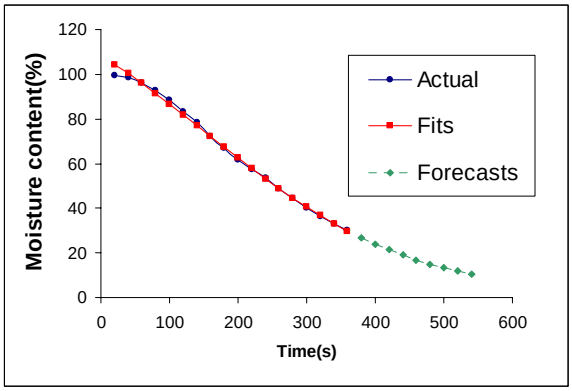

Figure 2.3. Moisture content vs. time for pine, (Microwave drying).

Microwave drying generate heat from within the grains by rapid movement of polar molecules causing molecular friction and help in faster and more uniform heating than does conventional heating. It should be pointed out that by variation of drying conditions (i.e. air temperature, humidity and air velocity) within a lumber stack, it is expected that the drying rate and the moisture content distribution varies as well [10].

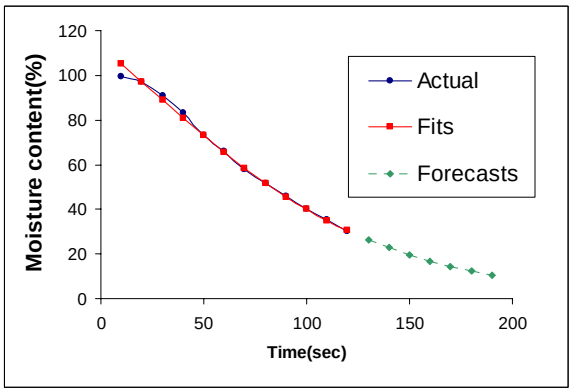

Figure 2.4. Moisture content vs. time for pine, (Combined dryer).

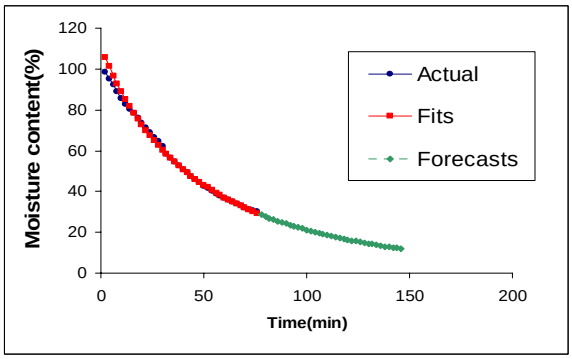

Figure 2.5. Moisture content vs. time for spruce, (Convection drying).

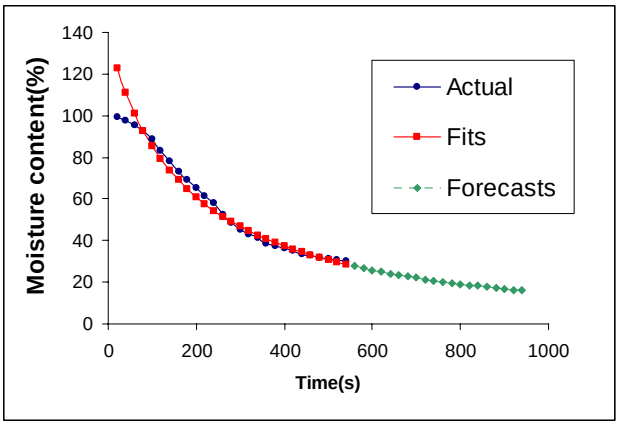

Figure 2.6. Moisture content vs. time for spruce, (Microwave drying).

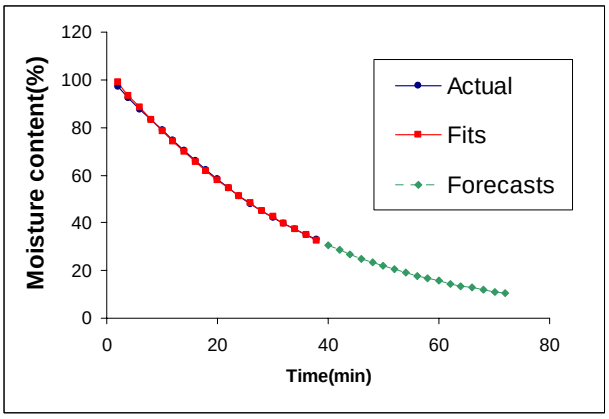

Figure 2.7. Moisture content vs. time for Spruce, (Infrared drying).

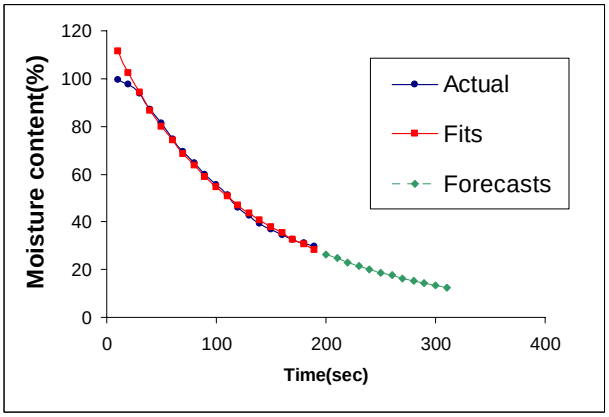

Figure 2.8. Moisture content vs. time for spruce, (Combined dryer).

The method of drying, type of samples, Mean Absolute Deviation, Mean Absolute Percentage Error, Mean Squared Deviation of these models used for moisture content change with time are presented in table 2.1.

Table 2.1. Results of fitness

Type of Samples	Drying methods	MAPE	MAD	MSD
pine	Convection	0.341876	0.221418	0.080966
	Microwave	1.08315	0.86600	2.08191
	Infrared	1.07610	0.83372	2.51506
	Combined	1.26813	1.00335	3.72067
spruce	Convection	1.61692	1.16996	4.21973
	Microwave	4.8156	3.3411	33.2286
	Infrared	0.638023	0.420579	0.342695
	Combined	2.46335	1.63377	9.40387

It is clear that the MAPE, MAD, MSD values of this model were changed between 0.34-4.8, 0.22-1.63 and 0.08-33.22 respectively. As it can be seen for pine samples the convection method has a better fitness to the model and for spruce infrared drying model fitted the experimental data properly.

The estimated values are based on data from [11] and can be conveniently used for theoretical approach are shown in table 2.2.

It was assumed that the diffusion coefficient bellow FSP can be represented by [11]:

$$D = A.e^{\frac{-5280}{T}}.e^{\frac{Bu}{100}} \tag{2.11}$$

Where T is the temperature in Kelvin, u is percent moisture content, A and B are experimentally determined.

Drying time is calculated from theoretical approach and evaluated model. Results show that real time had best agreement with which was obtained from equation (10) while there was a significant difference between real time and the one obtained from equation (5). Some authors have assumed that the diffusion coefficient depends strongly on moisture content [12-14] while others have taken the diffusion coefficient as constant [15-18]. Also, different boundary conditions have been assumed by different authors [19-22]. But Liu. et al concluded that the diffusion coefficient is a function of time, position, moisture content, and moisture gradient, which is at variance with assumptions in the literature that the diffusion coefficient is either a constant or a function of moisture content only [23].The difference in drying time may be due to the fact that diffusion coefficient was assumed to be the same in tangential and radial direction. So this assumption can't be used for equation (5). The same calculation can be done for other drying methods to predict the drying time.

Table 2.2. Set of data selected for this study

Specifications	value	Reference
S_x	2.9cm	[11]
S_y	10.2cm	[11]
u_0	82.5%	[11]
u_{eq}	16.2%	[11]
$\bar{u}$	19%	[11]
T	316.15K	[11]
α	$0.787\times10^{-5} cm/s$	[11]
D	$8.711\times10^{-6} cm/s$	Equation(11)
β_x	1.3099	Equation(7)
β_y	4.6072	Equation(7)
μ_x	0.925	Equation(6)
μ_y	1.2676	Equation(6)
Γ_x	0.99	Equation(8)
Γ_y	0.985	Equation(8)
A	$11.7cm^2/s$	[11]
B	$3.14cm^2/s$	[11]
t	213hr	Equation(5)
t	557.32hr	Equation(10)
t	420hr	Trend analysis
t (real time)	550hr	[11]

2.4. CONCLUSION

Selection of the optimum operating conditions to obtain good quality dried products requires knowledge of the effect of the process parameters on the rate of internal-external mass transfer. High temperature heat treatment of wood is a complex process involving simultaneous heat, mass and momentum transfer phenomena and the effective models are necessary for process design, optimization, energy integration, and control.

Infrared heating offers many advantages over conventional drying under similar drying conditions. These results in high rate of heat transfer compared to conventional drying and the product is more uniformly heated rendering better quality characteristics. Microwave drying offers a number of advantages such as rapid heating, selective heating and self-limiting

reactions which in turn can lead to improved quality and product properties, reduced processing time, and energy consumption and labor savings.

For pine samples the convection method has accurate result to the model and for spruce infrared drying model fitted the experimental data properly, thus their model was found to be adequate in predicting drying time of wood samples under different drying methods. The principle reason for drying wood at higher temperatures is because the rate of diffusion increases with the temperature. Water molecules generally diffuse from a region of high moisture content to a region of low moisture content, which reduces the moisture gradient and equalizes the moisture content. Diffusion plays an important role in the drying of lumber, at all moisture content with impermeable timbers and in permeable timber wherever the moisture content is too low for hydrodynamic flow of water through the lumens. Diffusion coefficient is influenced by the drying temperature, density and moisture content of timber. Other factors affecting the diffusion coefficient that are yet to be quantified are the species (specific gravity) and the growth ring orientation.

REFERENCES

[1] Perre. P., Turner. I.W., The use of numerical simulation as a cognitive tool for studying the microwave drying of softwood in an over-sized waveguide, *Wood Science and Technology*, 33, 1999, 445–446.

[2] Rosen H.N., Drying of wood and wood products. In: Mujumdaar A.S. (ed.): Handbook of Industrial Drying. Marcel Dekker Inc., New York: 1987, 683-709.

[3] Plumb O.A., Spolek G.A., Olmstead B.A., Heat and mass transfer in wood during drying. *Intern. J. Heat Mass Transfer*, 28(9), 1985: 1669-1678.

[4] Stanish M.A., Schajer G.S., Kayihan F. A mathematical model of drying for porous hygroscopic media. *AIChE J*. 32(8): 1986, 1301-1311.

[5] Pang S. Moisture content gradient in softwood board during drying: simulation from a 2-D model and measurement. *Wood Science and Technology*. 30, 1996, 165-178.

[6] Pang S., Relationship between a diffusion model and a transport model for softwood drying. *Wood and Fiber Science.* 29(1), 1997, 58-67.

[7] Naghashzadegan. M., Haghi. A.K., Amanifard. N., Rahrovan. Sh., Microwave drying of wood: Prductivity improvement, *Wseas Trans. on Heat and Mass Transfer*, Issue 4, Vol.1, 2006, pp. 391-397.

[8] Pavlo Bekhta, Igor Ozarkiv , Saman Alavi, Salim Hiziroglu, A theoretical expression for drying time of thin lumber, *Bioresource Technology*. 97, 2006, 1572–1577.

[9] Sergovskii, P.S., Heat Treatment and Preservation of Timber, unpublished report, Moscow, Russia, 1975, p 400.

[10] Pang, S. "Airflow reversals for kiln drying of softwood lumber: Application of a kiln-wide drying model and a stress model", Proceedings of the 14th International Drying Symposium, vol. B, 2004, pp. 1369-1376.

[11] Baronas,F. Ivanauskas,M. Sapagovas, R., Modelling of wood drying and an influence of lumber geometry on drying dynamics, *Nonlinear Analysis: Modelling and Control, Vilnius,* IMI, No 4, 1999, pp.11-22.

[12] Meroney, R.N., The State of Moisture Transport Rate Calculations in Wood Drying, *Wood Fiber,* 1(1), 1969, pp. 64–74.

[13] Simpson, W.T., Determination and Use of Moisture Diffusion Coefficient to Characterize Drying of Northern Red Oak, Wood Science and Technology, 27(6), 1993, pp. 409–420.

[14] Skaar, C., Analysis of Methods for Determining the Coefficient of Moisture Diffusion in Wood, *Journal of Forest Products Research Society,* 4(6), 1954, pp. 403–410.

[15] Avramidis, S. and Siau, J.F., An Investigation of the External and Internal Resistance to Moisture Diffusion in Wood, *Wood Science and Technology,* 21(3), 1987, pp. 249–256.

[16] Droin, A., Taverdet, J.L. and Vergnaud, J.M., Modeling the Kinetics of Moisture Adsorption by Wood, *Wood Science and Technology,* 22(1), 1988, pp. 11–20.

[17] Mounji, H., Bouzon, J. and Vergnaud, J.M., Modeling the Process of Absorption and Desorption of Water in Two Dimension (Transverse) ina Square Wood Beam, *Wood Science and Technology,* 26(1), 1991, pp. 23–37.

[18] Soderstro¨ m, O. and Salin, J.G., On Determination of Surface Emission Factors in *Wood Drying, Holzforschung,* 47(5), 1993, pp. 391–397.

[19] Crank, J., The Mathematics of Diffusion, Chap. 9, 2nd ed., ClarendonPress, Oxford. 1975.

[20] Plumb, O.A., Spolek, G.A. and Olmstead, B.A., Heat and Mass Transfer in Wood during Drying, *International Journal of Heat and Mass Transfer,* 28(9), 1985, pp. 1669–1678.

[21] Salin, J.-G., Mass Transfer from Wooden Surface and Internal Moisture Non-equilibrium, *Drying Technology,* 14(10), 1996, pp. 2213–2224.

[22] Hukka, A., The Effective Diffusion Coefficient and Mass Transfer Coefficient of Nordic Softwoods as Calculated from Direct Drying Experiments, Holzforschung, 53(5), 1999, pp. 534–540.

[23] Jen Y. Liu, William T. Simpson, and Steve P. Verrill, An inverse moisture diffusion algorithm for the determination of diffusion coefficient, *Drying Technology,* 19(8), 2001, 1555–1568.